NTNU – Trondheim
Norwegian University of
Science and Technology

Effect of Residual Stresses on Fracture Resistance of Arctic Structures

William Magnor

Mechanical Engineering
Submission date: June 2013
Supervisor: Mons Hauge, IPM

Norwegian University of Science and Technology
Department of Engineering Design and Materials

Effect of Residual Stresses on Fracture Resistance of Arctic Structures

Student
William Magnor
NTNU

Supervisor
Professor Mons Hauge
Statoil

June 10, 2013

Abstract

In integrity assessments, residual stresses have a significant effect on the crack driving force. In fracture assessments according to BS 7910 residual stresses are treated conservatively, and is often assumed to be equal to the material yield strength. In this work, a finite element model of a cracked steel plate was used to study the contribution to crack driving force from residual stresses. Residual stresses were introduced by the eigenstrain method and nodes were released to create cracks. Crack depths, a, up to 20 mm, crack lengths, $2c$, up to 50 mm and through thickness cracks were investigated. Solutions were compared to reference solutions with the same crack dimensions, but no residual stress. Corresponding fracture assessments according to BS 7910 were performed to illustrate the difference in crack driving force between FEM and BS 7910. The dimensionless parameter R, was developed during this work and denotes the effect of residual stresses. R can be computed both for results from FEM and BS 7910. It can be seen that R depend on crack parameters and decrease as load increase. Generally, R is significantly higher for solutions according to BS 7910.

Sammendrag

Restspenninger spiller en betydelig rolle i integritetsvurderinger i form av birdag til den sprekkdrivende kraft. I bruddvurderinger etter BS 7910 behandles restspenninger konservativt, og er ofte antatt å være lik materialets flytegrense. I dette arbeidet ble en elementmodell av en plate med sprekk ble brukt for for å undersøke effekten av restspennigner på den drivende kraft. Restspenninger ble innført i analysen ved bruk av eigenstrain metoden, sprekker ble dannet ved å slippe opp noder. Sprekkdybder, a, opp til 20 mm, sprekklengder, $2c$, opp til 50 mm og gjennomgående sprekker ble undersøkt. Løsninger er sammenlignet med referanseløsninger med samme sprekkdimensjoner uten respspenninger for å illustrere effekten av restspenningene. Løsninger for de samme tilfellene er utarbeidet i henhold til BS 7910 for å sammeligne BS 7910 med FEM. Den dimensjonsløse parameteren R er innført i dette arbeidet og betegner effekten av restspenninger. R kan regnes ut både ut ifra BS 7910 of FEM. Det viser seg at R avhenger av sprekkens dimensjoner og minker når den ytre lasten øker. R er i de fleste tilfeller betydelig høyere for løsninger etter BS 7910.

Contents

1 Introduction

In this section the motivation for the work performed will be briefly presented as well as a brief overwiev of material, design and fracture assessment standards taking residual stresses into account. Previous work on the subject will also be presented.

1.1 Background

This Master's thesis is written based on findings of previous work[1] by the same author. The aim is to investigate the effect of residual stresses on fracture resistance of Arctic structures. Findings may be appliccable to other welded structures as well. In many existing material and design standards residual stresses are treated in what is believed to be a conservative manner, especially considering the effect on fracture behavior. As the risk of cleavage fracture increases, at lower temperatures, materials are often difficult to qualify for application in the Arctic region. If better knowledge of residual stresses and their effect on fracture resistance were to be obtained, better utilisation of load capacity of welded structures would be possible and explorations of oil and gas in the Arctic area more cost-efficient[2, 3]. Safe and reasonably conservative treatment of residual stresses would also be preferrable in other areas than sturctures specifically build for the Arctic. In order to develop more realistic and less conservative rules and guidelines for structures applied in the Arctic, action has been taken. E.g. the execution of project Arctic Materials, as described in Section 1.2.

1.2 Arctic Materials

Estimates show that as much as 25% of the world's total remaining oil and gas resources may be located in the arctic area[4, 5]. At design temperatures down to $-60°C$, fracture toughness of structural steels are often severely lowered. Thus, common sturctural steels are often very difficult to qualify for application at such low temperatures according to existing material and design standards. E.g. ISO 19902[6], which states Charpy requirements for temperatures down to $30°C$ below the lower anticipated service temperature (LAST). In practice, this is requirement is very difficult to meet. NS-EN 10025[7] dictates Charpy requirements at temperatures down to $-50°C$. Charpy testing is a low-cost and effective way of indicating fracture toughness, however the testing values are somehow difficult to use in fracture assessments. As fracture resistance is often the limiting factor, residual stresses play a crucial role. In 2008 SINTEF carried out a five year research and development project, which ended late 2012. The Project was named Arctic Materials and NTNU and many major industries participated. The overall goal was;

"to establish criteria and solutions for safe and cost-effective application of materials for hydrocarbon exploration and production in arctic regions" [8]

This project has been of great importance with respect to describing properties of various steels, welds, polymers and composites at lower temperatures[9]. Based on findings of this project, a guideline was developed[10] in order to provide the industy with recommendations for materials qualification and selection in the Arctic. In terms of weld qualification the requirements for CTOD are based on fracture assessment according to BS 7910 in the guideline.

1.3 Arctic Materials II

After Arctic Materials I was finished late 2012, there was recognized that there still is a need for further research on this subject. Hence, there is motivation for continuing this work and developing guidelines and solutions for application in the Arctic. The scope for Arctic Materials II is prepared, as well as an estimated cost plan[9]. Residual stresses is among the areas that will be further investigated, given financial support. Both experimental testing and numerical modelling are among the tasks that will be executed in order to quantify the effect of residual stresses on structural integrity.

The contribution to crack driving force from residual stresses are, according to current standards, often assumed equal to the material yield stress. However, the real contribution is unknown. This assumption is believed to be exessively conservative, hence there is a potential for relaxation. Even though some standards, e.g. BS 7910[11], allows a slight relaxation there is probably a greater potential, i.e. the assumed crack driving force at a given load on a cracked component is probabily lower than what is assumed in BS 7910. Hence, there might be a potential for futher relaxation. Still, there is a need for tangible evidence and quantification of the effect of residual stresses on fracture resistance. Providing such information is the aim of this work.

1.4 BS 7910

Bristish Standard, BS 7910 - "Guide to methods for assessing the acceptability of flaws in metallic structures"[11], is one of the most common standards used for integrity assessments. The main focus is on flaws in welded structures consisting of ferritic or austenittic steel or aluminium alloys, but it is also apliccable for sturctures that are not welded. The approaches presented in BS7910 are apliccable both in the design, fabrication and operational phase of a structures life, e.g. the use of a failure assessment diagram, which takes both brittle and ductile fracture into account. The general assumption in BS 7910 is that residual stresses

are equal to the material yield strength, in contributing to the stress intensity factor, K_I, with a relaxation as the load increases to a certain level. It is notet that this might be conservative, and suggestions on stress distributions are given. However, these are upper bound values based on experiments. Hence, there is great motivation for investigating the effect of residual stresses on fracture resistance. Especially for structures applied in the Arctic, where fracture toughness often is the limiting factor. The parts of BS 7910 which are relevant for this work will be presented more thoroughly later.

1.5 Previous work

It is a common notion that residual stresses are treated conservatively in fracture assessments, e.g. according to BS 7910. Hence, previous research work has focused on this subject. Research has indicated that external loading may reduce the crack tip constraint, i.e. lowering the contribution from residual stresses on the crack driving force as external load increase[12, 13, 14]. Work as also indicated that residual stress profiles outlined in BS 7910 cause significanly negative T-stresses along the crack front, which in practice leads to increased fracture resistance[15]. As fracture assessments can be sensitive to the residual stress profile through the thickness of a plate or pipe, there is motivation for further investigation on the effect of residual stresses on the crack driving force.

1.6 Scope of this work

The scope if this work is studying the effect of residual stresses on fracture resistance. The core of this study is the use of finite element anaylses (FEA) to determine this effect. Residual stresses were introduced in FEA by the eigenstrain method which will be presented later. The material used was a 420 MPa steel used in project Arctic Materials. Releasing nodes to create cracks and applying load will result in a crack opening displacement (CTOD) that can be calculated from the analyses. Different crack depths, lengths and shapes were analysed. Reference solutions without residual stress were used for comparison. The scope was limited to crack in the weld centre. The dimensionless parameter, R, which among others depend on crack length, crack depth and load, was established in order to quantify the effect of residual stresses. Results were compared to integrity assessment according to BS 7910.

2 Theoterical background

In this section there will be given a brief introduction to the theoretical aspects to be considered when studying residual stress and it's effect on fracture behavior. Different methods of measuring residual stresses will also be presented.

2.1 Micromechanisms during welding

The aim of this section is to briefly illustrate the complex mechanisms that occur in a material during welding, and result in residual stresses.

2.1.1 Thermal expansion and contraction

When welding a plate, pipe or any other component, the weld metal must be heated to above the melting point. Heating the weld metal causes a number of material parameters to change temporarily. The most obvious parameter that changes during a welding heat cycle is the mass density. This due to thermal expansion/contraction, i.e. the volume increase when heating and vise versa. After cooling below the melting point, the weld metal is "fixed" to the base material. Hence, contraction will be restrained by the base metal. This cause tensile stress in the weld bead and compressive stresses in the near base metal, longitudinal to the welding direction. Likewise, the metal will contract in three dimensions. Therefore, a residual stress field with stresses in all three directions is created.

2.1.2 Phase transformation during welding

Volume changes are not solely caused by thermal expansion or contraction. Common structrual steels consist mostly of ferrite, i.e. body-centered cubic crystal structure. Ferrite is stable below $\sim 900\ ^\circ$C. Above this temperature, austenite is stable, having face-centered cubic crystal structure and is more dense than ferrite. Residual stresses are for the most part caused by austenite to ferrite transformation during cooling below $\sim 900^\circ$C. Some steels are austenittic at room temperature. Hence, residual stresses in austenitic and ferritic steels are different. Other factors, e.g. heating/cooling rate, also affect the phase transformation which indirectly affect the distribution of residual stresses.

2.1.3 Other considerations

As temperature increase, yield strength decrease and vice versa. Hence, the material yield more easily at higher temperatures. This change in yield strength probabily realx the residual stress magnitude. As different effects that occurs

during welding are added, it can be seen that residual stresses is not a straightforward problem. Residual stresses are rather the sum of a number of non-linear effects. Thus, simplifications are made in intergrity assessments.

2.1.4 Simplified determination of residual stresses

A Saoth-test can be used in order to demonstrate the result of the different effects that occurs during a weld thermal cycle. Satoh-testing means clamping a test specimen with given geometry in both ends, heating it and measuring the axial reaction force in one end, as showed in Fig. 1. Tensile/compressive force are measured and a $\sigma - T$ curve can be plotted as in Fig.2. In a real weld however, the conditions are different. Still, this test give an indication of the potential residual stresses that can occur in a welded component of the same material.

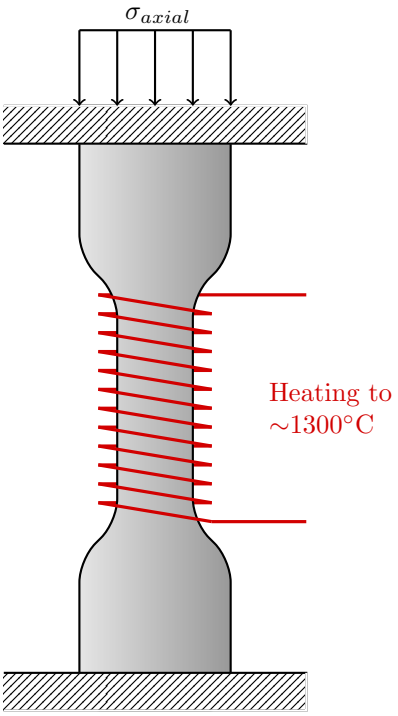

Figure 1: Rough sketch of Satoh-test set up[16]

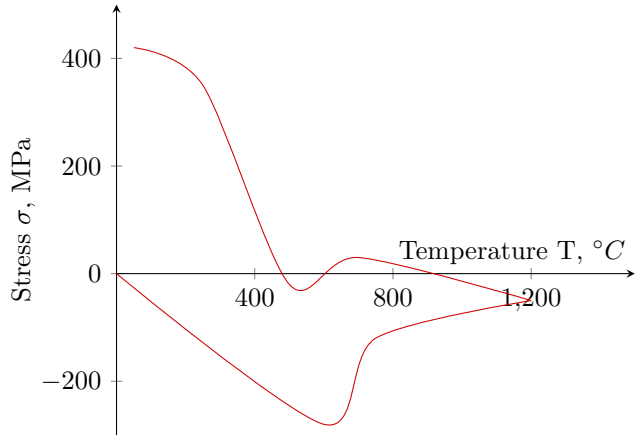

Figure 2: Typical Satoh test result[16]

2.2 The finite element method

In this section, finite element method (FEM) will be presented very briefly. In order to detemine approximate distributions of stresses, strains and displacements in a structure, FEM can be applied. FEM is a numerical technique which also can be applied in other areas than structural analyses. Currently, this is often the preferred method in sturctural analyses. In brief, FEM is used in determining an approximatie solution of a complex problem, by discretization of the component into finite elements with known solutions.

2.2.1 Key concepts

First, the geometry of the model is defined and then diveded into discrete regions, known as elements. Material properties, loads and boundary conditions (BCs) are assigned to the elements. The elements are connected by nodes which can be assigned with different degrees of freedom (DOFs). Different element types are available having different shapes, shape functions, number of nodes and number and types of DOFs. DOFs are mainly roatations and translations, e.g. translation in x-direction, denoted U1, and rotation around the y-axis, denoted UR2. The model is finally solved, using known deformation fuctions for the elements. This is an approximate solution, analogous to the idea that a large number of connected straight lines will form a curve and the sum of the length of each line is equal the length of the curve. At nodes with BCs assigned, the deformations are known. As elements are connected via nodes, deformation, stresses, etc. at these points are transferd to the next element. Hence, the computer solves a set of equations where the unknowns are solved via deformation functions of the elements. If accurate results are needed, there might be a need for dividing the model into a large number of elements. Is such cases, the numer of equations for the computer to solve may be in the hundreds of thousands or even millions. Hence, very powerful computers are often necessary to perform such analyses within an accepable timeframe.

2.2.2 FEM in structural analysis

As noted, different element types are available. In structural analysis solid elements are often used, but other elements such as beam and shell elements are also available. In this work, mostly solid, but also shell elements were used. As noted, deformation functions define the deformation of an element when a load or displacement is applied, e.g. the stresses can be assumed linear between each node if the deformation function is linear. Therefore, if accurate results are needed, the mesh needs to be fine, i.e. small elements. However, as number of elements and accuracy of results increase, the number of equations and unknowns

increase. Hence, computational time and the amount of data that is written increases. A trade-off must be made between accuracy of results and computational time and data written. Therefore, FEM tools usually allow different regions to be assigned with different element size, i.e. fine mesh where accuracy is important, and coarser in areas where accurate results are not of importance. It is relevant to mention, however, that the supercomputer Vilje on NTNU was available. Therefore, analyses with high number of elements could be solved quickly and less attention was paid to reducing computational time.

2.3 Determination of residual stresses

As stated above, residual stresses are caused by inherent strain in the material. Here inherent strain means strain caused by the welding thermal cycle. In literature the terms inherent strain and eigenstrain are both used, from here on the term eigenstrain will be used. The residual stress distribution is among others determined by the distribution of eigenstrain and geometry of the welded component. Other factors, as e.g. the heat input, may also affect the distribution of residual stresses. The latter may have a crucial impact on the distribution over the thickness of a welded plate[11, Fig. Q.1]. In litterature, stress distributions vary siginificantly[17]. As a lot of variables impact the residual stress distribution, there is difficult to determine a general solution.

2.3.1 Determination by neutron diffraction

Neutron diffraction is a non-destructive method, which can be used for determining stresses in crystalline materials. This method is applicable for determining residual stress- and strain distribution in a welded component[18, 19, 20]. However, this method is limited to determination of residual stresses in a laboratory, i.e. on smaller specimens meant for laboratory experiments. Hence, it is not applicable for use on welded structures. Still, it can prove useful in terms of giving an indication of the residual stresses in a weld. However, the geometry of an actual structure may alter the residual stress distribution. Hence, caution must be taken and geometry conditions considered carefully.

2.3.2 Destructive methods for determining residual stresses

There are also a number of destrictuve methods for determining residual stresses. With the use of strain gauges, the residual stresses in a welded plate, or other component, can be determined. The methods are based on removing material from the weld zone in a welded test plate, by e.g. drilling holes at different angles or slicing a welded plate. The change in strain can then be measured from the strain gauges and a stress field can be constructed based of this.

2.3.3 Eigenstrain in FEM

Due to complexity, especially during phase transformation, it is difficult to predict a residual stress field using conventional FEM tools. Still, software has been developed, e.g. WeldsimS[21], which can determine the residual stress field in a steel weld. On the other hand, this is very time consuming, especially when multi-pass welding is simulated, which is often the case in real life. A different and simpler method is introducing eigenstrain in FEM by using thermal expansion. This can be done with conventional FEM tools as ABAQUS and is the method used in this work, i.e. WeldsimS in not used.

As the residual stress in a weld can be determined with e.g. neutron diffraction, this stress field can be introduced in conventional FEM tools using the eigenstrain method. The magnitude of the eigenstrain in a weld is usually relatively high close to the weld and lower farther away[18]. Assigning the weld- and parent material with different thermal properties, then changing temperature will result in a strain- and associated stress field. This is a simplyfied approch, as the distribution of eigenstrain is continous in a real weld. Note that the thermal expansion coefficients that are assigned are not supposed to be the same as in real life, but rather fictious values, assigned in order to create the desired stress field. Changing the thermal expansion coefficient and geometry is done in order to change the stress field. This method however, requires some knowledge about the residual stress field from e.g. experiments. Still BS 7910 gives indications on how the shape of this stress field, in annex Q figure Q.1. Here it can be seen that there are often tensile stresses in the surface and compression in the middle, in welded plates transverse to the welding direction. The scope of this work includes cracks in the symmetry plane of a weld, with tension loading transvere to the crack and welding direction.

2.4 Fracture mechanics theory

If a plate, pipe or other component contains a crack, the component may show brittle fracture behavior even though the material is ductile, as e.g. structural steels. Fracture mechanics theory is a very comprehenive field of study and can be used to describe brittle failure mechanisms. Usually, residual stresses are not taken into account in design as they don't contribute to failure when a crack is not present[22, section 9.1.4]. However, residual stresses contribute to the crack driving force, crack tip constraint, etc. once a crack is introduced in an area where residual stresses are present. Therefore, it is relevant to present how residual stresses are introduced in fracture mechanics theory.

2.4.1 Classical fracture mechanics

Classical fracture mechanics theory view the fracture toughness as a single parameter determining whether or not fracture will occur. This is analogous to the Mises stress determining if the material will yield. Fracture can occur both in the elastic and plastic area. Hence, linear elastic- (LEFM) or elastic-plastic fracture mechanics (EPFM) can be used to assess fracture in their respective areas of application[22]. Theory in both areas are well established and implemented in common standards. Mainly, there are three different measures of the crack driving force. K, is used in LEFM while J and δ is valid for EPFM under small scale yielding and larger scale yielding respectively. In FEM tools, the crack driving force can usually be determined directly. In this work CTOD, denoted δ, is used as the crack driving force, being valid under both small and large scale yielding. CTOD is also widely used in standards.

In BS 7910, the contribution from residual stresses on stress intensity, K_I, are treated in the same manner as a contribution from an external load, i.e. the effects are added. This will be elaborated later.

2.4.2 Elastic-plastic fracture mechanics

In LEFM, the crack driving force, K, is given by crack depth, crack geometry and applied load. This is shown in Eq. (1) where σ is that applied stress, a is the crack depth and f is a geometry factor. The index I denotes mode I loading, which means loading normal to the crack plane. Note that Eq. (1) may have different formulations. It can be seen that K_I is linearly dependent on the applied stress. However, as plasticity at the crack tip becomes more widespread as load increases, the effective crack driving force increase more than what LEFM predicts. Hence, K_I is no longer valid. This is shown in Fig 3[22, Fig. 9.18]. This is relevant in terms of fracture assessments and is taken into account in BS 7910 which is presented later.

$$K_I = f * \sigma\sqrt{\pi a} \tag{1}$$

2.4.3 J-Q theory

Classical fracture mechanics theory view fracture toughness as a single material parameter. When the applied crack driving force reaches the critical value, e.g. δ_{mat} or K_{crit}, brittle fracture occurs. However, this is proven to be valid only under small scale yielding. Due to plastic deformation at the crack tip when loading, the crack tip constraint decrease. The parameter Q is defined as the amplitude of the shift in the stress field caused by constraint loss at the crack

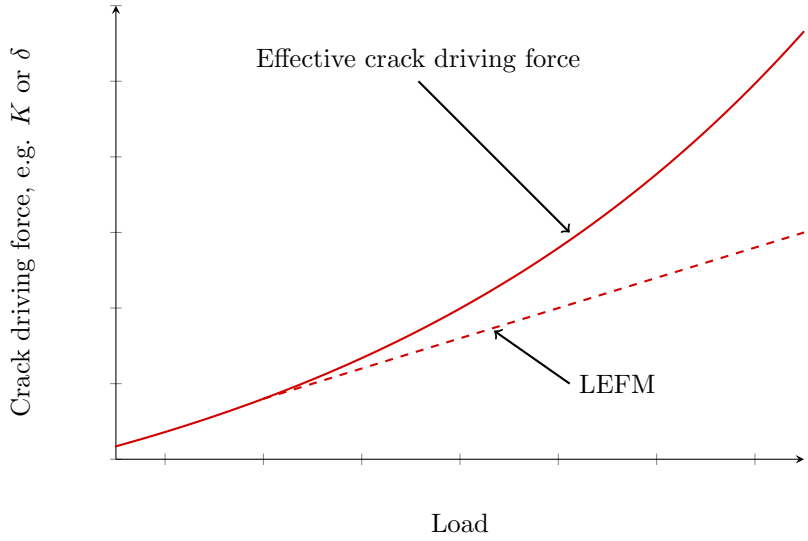

Figure 3: LEFM vs effective crack driving force

tip. Q is uniquely related to the T-stress and $Q = 0$ on the limit to small scale yielding. Q is always negative when T is negative and vice versa. The so called J-Q theory[22, 3.6.2] has been developed take this effect into account. For laboratory specimens, T is given by Eq. (2), where β is the biaxaiality ratio and depend on geometry.

$$T = \frac{\beta P}{B\sqrt{\pi a W}} f\left(\frac{a}{W}\right) \tag{2}$$

Center cracked tension (CCT)- and double edge notch tension (DENT) specimens are cases where $\beta < 0$, i.e. $T < 0$, for all a/W ratios up to 0,2 and 0,8 respectively. While $\beta < 0$ for SENT and SENB specimens, until the a/W ratio reaches ∼0,6 and ∼0,35 respectively[22, fig 3.34]. Note that for a through thickness crack in an infinitely wide plate, $\beta = -1$ for mode I remote loading. Which is approximately the case for CCT specimens with a/W below 0,2.

Further, assuming small-strain theory, the stress field well inside the plastic zone close to a crack tip is given by Eq. (3) where $(\sigma)_{T=0}$ is the stress field for $T = 0$ and δ_{ij} is the Kronecker delta. The second term is called the difference field which determines the shift in the stress field caused by constraint at the crack tip. Recall, Q, is uniquely related to T and always have the same sign.

As menioned, T and Q are uniquely related and the relationship depend on the strain hardening exponent, n, of the material considered. As $T = 0$ give $Q = 0$, $T = -1$ gives values of Q in the range $\sim -0,8$ to ~ -2 depending on n. However, if $T = 1$, Q range from $\sim 0,1$ to $\sim 0,4$. Hence, a decrease in T is more significant to Q than an increase of the same magnitude, from the same reference point[22, Fig. 3.35]. Cases where $T = 0$ are considered high constraint cases, like e.g. single edge notch bending (SENB), where $T = 0$ for $a/W \approx 0,35$[22, Fig. 3.34]. In realistic scenarios however, the constraint is often lower, i.e. T and Q are lower and the stress field inside the plastic zone is lower than the solution with a high value T.

$$\sigma_{ij} = (\sigma_{ij})_{T=0} + Q\sigma_0\delta_{ij} \quad \left(|\theta| \leq \frac{\pi}{2}\right) \tag{3}$$

2.4.4 Developments of the J-Q theory

J-Q theory has over the years been developed further, taking additional effects into account. As HAZ, weld- and base material often have different material properties, i.e. yield strength and strain hardening, the stress field close to a crack tip located near a weld is affected by this. Using a modified boundary layer model on a bi-material, the effect of mismatch has been included a similar manner as Q in Eq. (3), where the amplitude of the difference field is named M[23]. Hence, the name J-Q-M theory. However, the effect of mismatch is not taken into account in this work.

Further, is has been shown that residual stresses can be taken into account in the same manner as Q and M[12], where R is the amplitude of the difference field cased by residual stresses. This was done by using a modified boundary layer, and including residual stresses using eigenstrain. It is shown that R is related to T, and that R decreases as T increase. In practice this means that increasing external load, the effect of residual stresses becomes smaller. This is in not necessarily in agreement with how residual stresses are treated in fracture assessments.

3 Residual stresses in material and design standards

In this section, an overwiev of how residual stresses are treated in Arctic materials KMB guideline and BS 7910 is presented. As noted, residual stresses are often treated conservatively in common material and design standards, and is frequently assumed to be equal to the material yield strength.

3.1 Arctic material KMB project guideline

In Arctic material KMB project guideline[10], which is based on the outcome of project Arctic Materials, specific requirements for CTOD on materials used are stated. On utilisation of up to 80% of the material yield strength, it is noted that residual stresses are of importance. However, the required CTOD toughness that is stated is based on residual stresses being equal to yield, with relaxation in accordance with BS 7910. Cracks with depths of 5 mm are assumed for all wall thicknesses[10, section 11]. This is based on fracture mechanics theory which means adding the contributions from residual stresses and external loading to the stress intensity factor, K.

3.2 BS 7910

BS 7910 - "Guide to methods for assessing the acceptability of flaws in metallic structures"[11] is a widely used standard for fracture assessments. Methods presented in BS 7910 are applicable in the design, fabrication and operational phases of a structure's life, and can be used for assessing the acceptability of an existing or postulated flaw.

3.2.1 FAD apporach

A common approach for determining whether or not a given crack pose a danger or not, is the use of a failure assessment diagram (FAD) and is used in BS 7910. Using this method, fully brittle fracture, fully plastic collapse and brittle fracture with prior plastic deformation are taken into account. On a FAD, the fracture ratio, K_r or $\sqrt{\delta_r}$, is plotted along the y-axis and the load ratio, L_r, is plotted along the x-axis. The load ratio determines the danger of plastic collapse and the fracture ratio determines the danger of brittle fracture.

3.2.2 Load- and fracture ratio

According to classical fracture mechanics, the crack driving force is a function of the applied load, i.e. fra fracture ratio is a function of the load ratio. As a cracked

component is loaded, each load ratio will have a corresponding fracture ratio, and a plot can be made, hereafter referred to as a load path, e.g. when assessing a severely cracked specimen, the load path is very steep. For an uncracked specimen the curve is coincident with the x axis. Eq. (4) to Eq. (7) describes how the fracture- and load ratios are detemined. Note that both K_r and $\sqrt{\delta_r}$ are equally valid measures of the fracture ratio. In Eq. (4) and Eq. (6), ρ is a correction factor for plasticity interaction between secondary and primary stresses. The formulation of ρ is given in annex R in BS 7910, where a simplified and detailed approach is given. The simplified approach is sufficient for cases investigated in this work, but the formluae will not be presented here. However, it can be mentioned that ρ is highest at zero load, decrease as load increase and is omitted when below zero. Eq. (5) is used for converting applied K_I to an equvivalent δ_I, where X usually between 1 and 2[11, 7.3.6.1].

$$\sqrt{\delta_r} = \sqrt{\frac{\delta_I}{\delta_{mat}}} + \rho \tag{4}$$

$$\delta_I = \frac{K_I^2}{X\sigma_Y E'} \tag{5}$$

$$K_r = \frac{K_I}{K_{mat}} + \rho \tag{6}$$

$$L_r = \frac{\sigma_{ref}}{\sigma_Y} \tag{7}$$

The reference stress, σ_{ref}, in Eq. (7) is the stress to be considered in terms of assessing plastic collapse in the crack ligament, and has different formulations for different crack geometries. This stress is computed according to Eq. (8) and Eq. (9) for through thickness and surface cracks respectively. Here, α'' is given by Eq. (10) for $W \geq 2(c+B)$ and by Eq. (11) for $W < 2(c+B)$. P_m and P_b are the membrane and bending stress, a the crack depth, c half the crack width, W the plate width and B the plate thickness.

$$\sigma_{ref} = \frac{P_b + (P_b^2 + 9P_m^2)^{0,5}}{3\left\{1 - \left(\frac{2a}{W}\right)\right\}} \tag{8}$$

$$\sigma_{ref} = \frac{P_b + \{P_m^2 + 9P_m^2(1-\alpha'')^2\}^{0,5}}{3(1-\alpha'')^2} \tag{9}$$

$$\alpha'' = \frac{\frac{a}{B}}{1 + \frac{B}{c}} \tag{10}$$

$$\alpha'' = \frac{\left(\frac{2a}{B}\right)}{\left(\frac{c}{W}\right)} \tag{11}$$

3.2.3 The assessment line

As mentioned, a load path can be plotted as a cracked component is loaded, e.g. from zero to a maximum load. In order to detemine whether or not this load is acceptable, BS 7910 yields formulae for the so called assessment line. Different formulas for level 1, 2 and 3 FAD analyses are given for different levels of accuracy. In this work, a level 2B assessment is performed, which is the normal assessment with material specific stress-strain data taken into account. The assesment line for level 2B is given by Eq. (12) and shown in Fig. 4. Note that the shape of the assessment line depends on the stress - stain curve of the material considered and Fig. 4 is a sketch, with roughly the same shape as for the material used in this work. Here, E is Young's modulus, ε_{ref} is the total strain and σ_Y is the yield strength. In cases where LEFM is valid, a single criterion, $K_r = 1$, would be sufficient in order to assess brittle fracture. However, this is rarely the case in real life. As shown in Fig. 3 the effective crack driving force is increasingly higher than what LEFM predicts at increasing load. The assessment line is designed to take account for the difference in driving force. Hence, the acceptable K_r becomes lower as L_r increase. The assessment line is usually cut of at $L_r = 1,15$ for low alloy steels and welds, which is relevant for this work. It can be seen from Fig. 4 that an assessment point easily can be judged either as acceptable or unacceptable.

$$K_r \text{ or } \sqrt{\delta_r} = \left(\frac{E\varepsilon_{ref}}{L_r\sigma_Y} + \frac{L_r^3\sigma_Y}{2E\varepsilon_{ref}}\right)^{-0,5} \tag{12}$$

3.2.4 Stresses to be considered

For fracture assessments, according to BS 7910, the stress intensity factor, K_I, is calculated analytically as in classical fracture mechanics. K_I is given by Eq. (13) which is a different formulation of Eq. (1). Here, $(Y\sigma)$ takes stresses and crack geometry into account and is analogous to $f * \sigma$ in Eq. (1). BS 7910 distinguishes between primary and secondary stresses. In Eq. (14), indexes p and s denote contributions from primary and secondary stresses respectively. In this work, residual stresses are treated as secondary and the external load as primary. This is in accordance wil BS 7910. Primary stresses contribute to both K_r and L_r and secondary stresses contribute to K_r, but not to L_r.

$$K_I = (Y\sigma)\sqrt{\pi a} \tag{13}$$

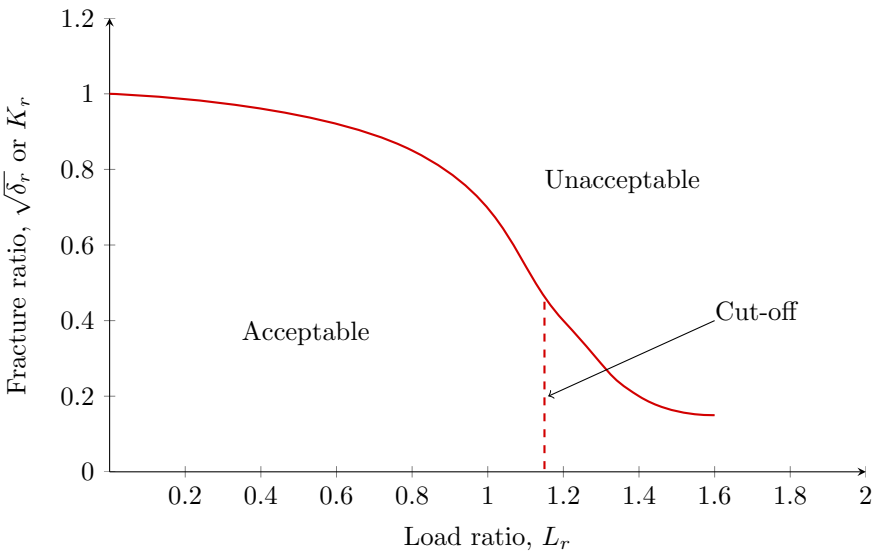

Figure 4: Failure assessment diagram level 2B

$$(Y\sigma) = (Y\sigma)_p + (Y\sigma)_s \tag{14}$$

3.2.5 Implementing residual stresses

In the case of residual stresses, they can either be assumed to be uniform or non-uniform. When the residual stresses are assumed to be uniform, they are assumed equal to the material yield strength, with a relaxation. The contribution from the residual stresses to K_I is then added to the contribution from the external loading. K_I is calculated according to Eq. (13) and Eq. (14). Where a is the crack depth and $(Y\sigma)$ is the contribution from primary and secondary stresses to the stress intensity factor, indexed p and s respectively.

For cracks that are parallel to the welding direction, the lower of the base and weld material yield strength shall be used. For this case, a relaxation of the residual stresses are allowed, according to Eq. (15), if not resulting in higher stresses than the yield strength, in which case Eq. (16) is used. Here, σ'_Y, σ'_f and σ_{ref} are the yield- and flow strength at assessment temperature and the reference stress, respectively. The flow stress is the average of the yield- and ultimate tensile strength. The reference stress is given by Eq. (8) and Eq. (9).

$$Q_m = \left(1,4 - \frac{\sigma_{ref}}{\sigma'_f}\right)\sigma'_Y \tag{15}$$

$$Q_m = \sigma'_Y \tag{16}$$

3.2.6 Non-uniform residual stress distribution

Assuming the residual stresses to be uniform over the thickness of a plate, however, is not realistic, as residual stresses are a self-equilibrating stress field. BS 7910 also allows the residual stresses to be assumed non-uniform, which is more realistic. In the case of non-uniform residual stesses however, relaxation according to Eq. (15) is not permitted. If known, the actual distribution of residual stresses can be used and alternatively linearized[11, Section 6.4.1]. Table 1 in BS 7910 gives guidelines on how to linearize a stress distribution, notifying that any linearization is acceptable as long as it is greater or equal to the real distribution over the crack surface. Linearization can be done e.g. according to Fig. 5 and Q_m calculated according to Eq. (18). If not known, the residual stress distribution may be taken from annex Q, which yield upper bound distributinos for different geometries. Eq. (17) for transverse residual stresses on flat plates, where z is distance from the surface and B the plate thickness.

$$\sigma_R^T = \sigma_Y[0,9415 - 0,0319(z/B) - 8,3394(z/B)^2 + 8,660(z/B)^3] \tag{17}$$

$$Q_m = \frac{\sigma_1 + \sigma_2}{2} \tag{18}$$

3.2.7 The resulting crack driving force

Further, $(Y\sigma)$ is calculated according to Eq. (14), where $(Y\sigma)_p$ and $(Y\sigma)_s$ are given by Eq. (19) to Eq. (22). For flat plates $M = M_m = M_b = 1$, while f_w is given by Eq. (20) for through cracks and by Eq. (21) for surface cracks. Where a is crack depth, W is plate width and B is plate thickness. M_m is given by crack geometry and varies along the crack front. The factors k_{tm}, k_{tb} and k_m take account for stress concentrations caused by the weld. The latter three are 1 in this work as the weld in FEM is completely planar and cause no stress concentration. P is the primary stress caused by external loading while Q is secondary/residual stresses. Indexes m and b represents membrane and bending components of P and Q.

$$(Y\sigma)_p = Mf_w(k_{tm}M_{km}M_mP_m + k_{tb}M_{km}M_b[P_b + (k_m - 1)P_m]) \tag{19}$$

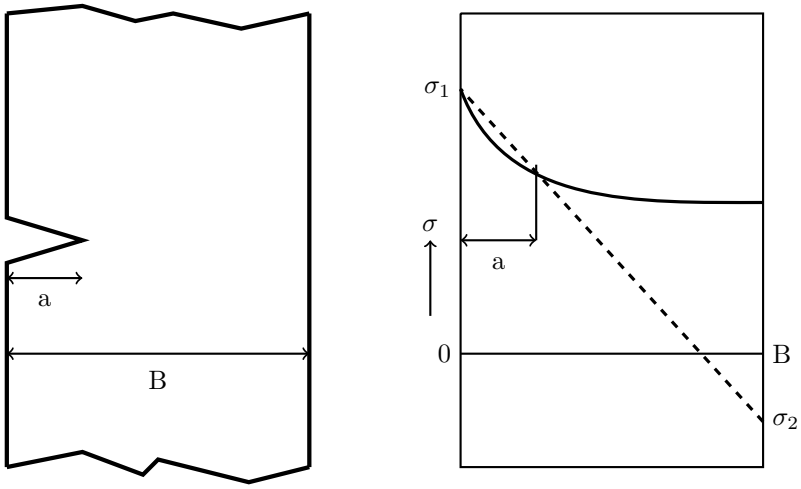

Figure 5: Example og linearization of stress field according to BS 7910

$$f_w = \left[sec\left(\frac{\pi a}{W}\right)\right]^{0,5} \tag{20}$$

$$f_w = \left[sec\left[\left(\frac{\pi a}{W}\right)\left(\frac{a}{B}\right)^{0,5}\right]\right]^{0,5} \tag{21}$$

$$(Y\sigma)_s = M_m Q_m + M_b Q_b \tag{22}$$

In the case of surface cracks, the stress intensity will vary over the crack front and is a function of the angle θ, which defines the position along the crack front. This is shown in Fig. 6. M_m is a function of the crack geometry, plate thickness and the position on the crack front. I.e. M_m is proportional to $f\theta$ which is a function of θ and is given in Eq. (23) for $0 \leq a/(2c) \leq 0,5$ and by Eq. (24) for $0,5 \leq a/(2c) \leq 1,0$. The entire function for determining M_m is given in BS 7910, M.3.2.2.2 and will not be presented here. It can be seen that $f\theta$ is constant over the crack front if $a = c$ and is equal to 1. However, the magnitude of residual stresses may vary over the crack front, i.e. the highest value of residual stresses must be considered for cracks with $a = c$ if a non-uniform distribution of residual stresses are assumed.

$$f\theta = \left[\left(\frac{a}{c}\right)^2 cos^2\theta + sin^2\theta\right]^{0,25} \tag{23}$$

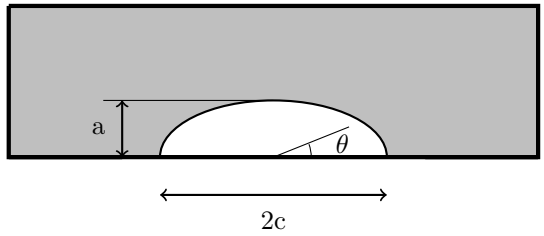

Figure 6: Surface flaw, dimensions according to BS 7910 Annex M

$$f\theta = \left[\left(\frac{a}{c} \right)^2 sin^2\theta + cos^2\theta \right]^{0,25} \tag{24}$$

4 Numerical analyses set-up

In this section the numerical investigation on the effect of residual stresses in fracture resistance will be presented. The purpose of this section is giving the reader insight in the method used and ensure re-producability of the analyses performed.

4.1 FEM tool - Abaqus/CAE

In this work Abaqus/CAE (Complete Abaqus Environment) was used for modeling and FEM analyses. Abaqus/CAE has a graphic user interface and allows a vast number of different simulation types. Being able to build a focused mesh in certain areas, Abaqus is well suited for fracture mechanic analyses, i.e. finer mesh can be built around the crack tip, where accurate results are required, and a coarser mesh in less interesting areas. Abaqus is also able to calculate the stress intensity factor, K_I and the energy release rate J, which are measures for the crack driving force, used in fracture mechanic analyses. However, CTOD was used in the work as the crack driving force. This due to K_I only being valid for linear elastic fracture mechanics (LEFM) and J only valid under small scale yielding. Here, CTOD is defined as the displacement og the node closest to the crack tip. This is assumed to be accurate as the elements aroud the crack tip are very small. In addition, the displacement of the node, closest to the crack tip was not sensitive to changes in the surrounding mesh, shown in Fig 10.

In Abaqus/CAE different modules are used for different tasks. The "Model" module is where the model is created. A plate is created by e.g. drawing and extruding, as was the method usen in this work. Dividing the model into different sections is also possible. Here, the weld was created as a section of it's own, as shown later. Defining material properties, relative position of different parts, interaction between parts, meshing, loading and running simulations are all performed in different modules in Abaqus/CAE.

In addition, input files can be written for each simulation. Once the input file is written, Abaqus can run the simulation only needing this file. This method was preferred in this work as multiple simulations, consisting of up to ∼300 000 elements, were run. The simulations were run simultaniously in bulks, on the supercomputer Vilje on NTNU.

4.2 Plate model

In this work, three different plate models were used. All 1200 × 1200 mm plates, with through thickness and surface cracks. The models with surface cracks

contained semi-elliptical cracks with both $a = c$ and $a \neq c$. All with thickness 25 mm. Hereafter, the plate with surface cracks with $a = c$, through thickness crack and surface cracks with $a \neq c$ will be referred to as model 1,2 and 3 respectively.

In order to avoid end effects, a crack needs to be small compared to the rest of the plate. End effects might alter the results, and what the simulation intends to show might come out unclear. All models were used assuming that surface cracks below the wall thickness are small enough to avoid end effects. All three models had two symmetry planes, i.e. only one fourth were modeled. This means that the dimensions mentioned above are twice the length and width of the simulated cases. In all cases, the cracks were located in the middle, to satisfy symmetry.

4.2.1 Plate and crack geometries

On model 1, crack depths up to 20 mm were created, assuming that the end effects were negligable. The same assumption was made for model 2, which was used for through thickness cracks. Here, the cracks were larger. On model 3, cracks with depth, $a = 5$ mm and length, 10 mm $\geq 2c \geq 50$ mm, were investigated. A 2D presentation of the plate models is shown in Fig. 7, while Fig. 8 shows the geometry of the seld in the FEM model. The weld had the same geometry in all cases investigated.

If a small surface crack is assumed to be semi-elliptical, the stress intensity factor is a function of the angle θ from the centre of the crack mouth opening, as shown in Fig. 6. For cracks with $a \leq 2c$, the crack driving force is greatest at the deepest point of the crack, given by Eq. (24). For cracks that are deeper than half the width, the crack driving force is greatest along the surface, given in Eq. (24). Over the course of fatigue, cracks will naturally grow at the highest rate, at the point along the crack front where the crack driving force is greatest. Given Eq. (23) and Eq. (24) and their applicable areas it can be seen that a crack will grow into a circular shape ($a = c$) over the course of fatigue. Hence, a crack grows through the plate when a crack reaches the plate thickness. Using the above assumption, that the crack is circular at this point, the width of the crack (2c) is twice the thickness. The crack can then conservatively be treated as a through crack, with length (2a) equal to twice the plate thickness. Therefore, in this work, through thickness cracks with length $2a \geq 50$ mm were investigated. It must be mentioned, however, that in practice the residual stress field has the potential of changing the shape of a fatigue crack. This due to the residual stresses being unevenly distributed through the thickness. However, studying this effect is not the focus area of this work.

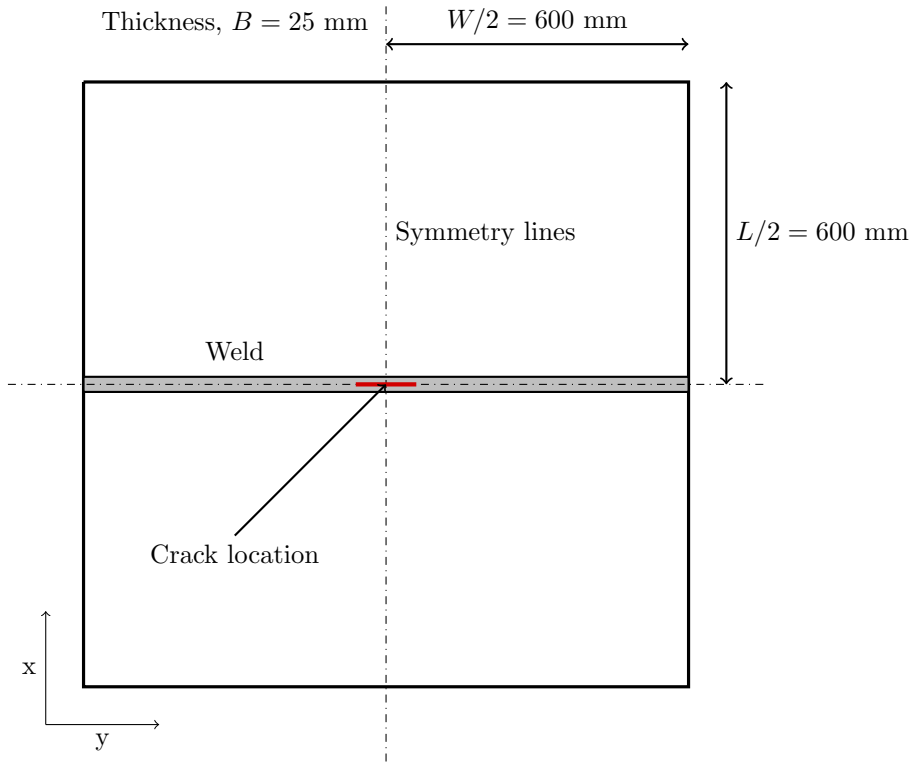

Figure 7: Plate model used in FEM simulations

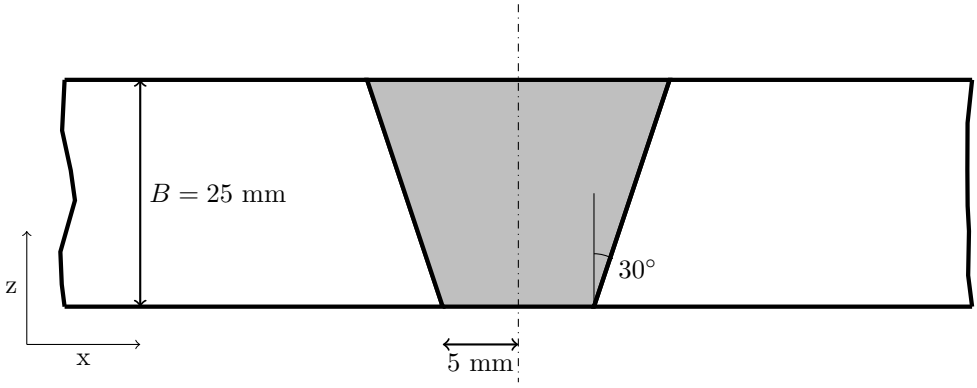

Figure 8: Close-up of weld

4.2.2 Material properties

As mentioned, different materials were assigned to the weld- and the base-section of the plate. Both having the same stress strain relationship, but different thermal expansion coefficients. Note that that thermal expansion coeficcients are not corresponding to those of the physical material considered, but values assigned in order to induce eigenstrain in the model. The base material was given an expansion coefficient of $\alpha = 0$ and the weld material was given $\alpha = 0,003$, the same values has been used in previous work[12]. The stress-strain curve is assumed equal to a 420 MPa steel being used in project Arctic Materials. Assuming The Ramberg-Osgood relationship, the stress-strain curve of the material i given by Eq. (25) which yields Eq. (26), where Young's modulus, $E = 207000$ MPa, ε is true strain and σ is the stress. However, this realtionship was implemented in Abaqus by plotting approx. 70 points on the curve. Eq. (25) is plotted based on this, using curve-fitting i Microsoft Excel, in order to present the stress strain relationship briefly here. The full stress-strain curve is found in Annex A. Further, it is relevant to mention that the Poisson coefficient was $\nu = 0,3$ and density was 7,8E-9 in the analyses. The flow strength was $\sigma_f = 1,1 * \sigma_Y$.

$$\frac{\varepsilon}{\varepsilon_0} = \frac{\sigma}{\sigma_0} + \alpha \left(\frac{\sigma}{\sigma_0}\right)^n \tag{25}$$

$$\varepsilon = \frac{\sigma}{E} + 650 * \sigma^{0,07} \tag{26}$$

4.2.3 Meshing

The model was meshed after being sectioned and seeding edges to get the desired element size at different areas. Seeding means assigning an edge with a given number of elements or given element size. The area around the crack, where accurate results were needed, was assigned with a very fine mesh, The element size was 0,1mm closest to the crack front, and increasing further away. Farther away from the crack, there were no need for such accurate results. Hence, a much coarser mesh was used in this area in order to reduce simulation time and the amount of data that is written.

As shown in Fig. 10 the mesh is very fine close to the crack tip, with element size decreasing further away. In an area 1×1 mm around the crack front the element size was smallest, i.e. $0,1 \times 0,1$ mm, while the length along the crack front was $\sim 0,3$ mm. The element size then increased to $\sim 0,5$ mm at distances $\sim 2,5 - 5$ mm away from the crack front. At further distance from the crack, the mesh was coarser.

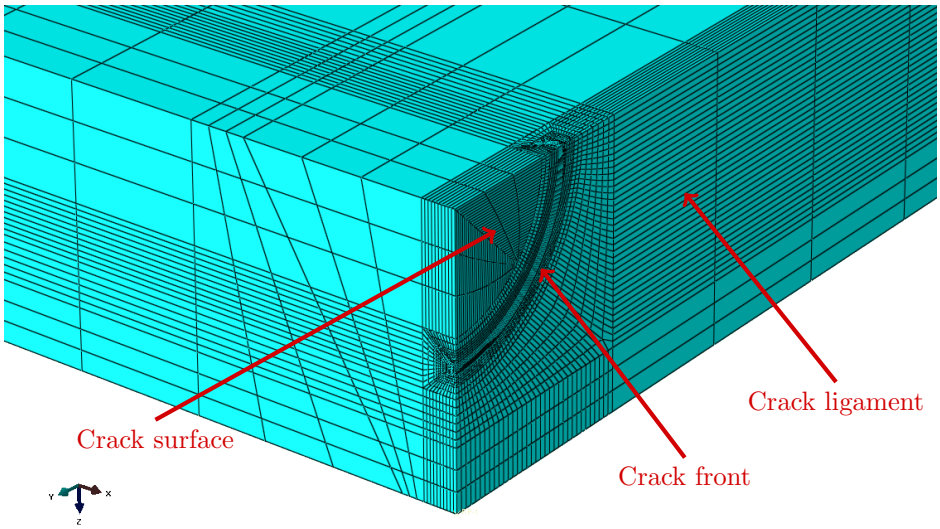

Figure 9: Mesh in crack and ligament area

The model was meshed, using cubic elements. The element type used was C3D8R, which is an eight node element with no rotational degrees of freedom, one integration point, and reduced integration.

4.3 Loading and boundary conditions

In Abaqus, loading and boundary conditions (BCs) can be applied stepwise. This allows for creating residual stresses, introducing cracks and applying loading separately, without interfering with each other. The main sequence of loading in this work, can briefly be summarized as;

- Initial step: Appropriate symmetry BC and BC hindering rigid body movement
- Step 1: Changing the temperature of the whole model in order to induce eigenstrain and create a residual stress field
- Step 2: Create crack by removing BC on crack surface
- Step 3: Applying load by adding a fixed displacement

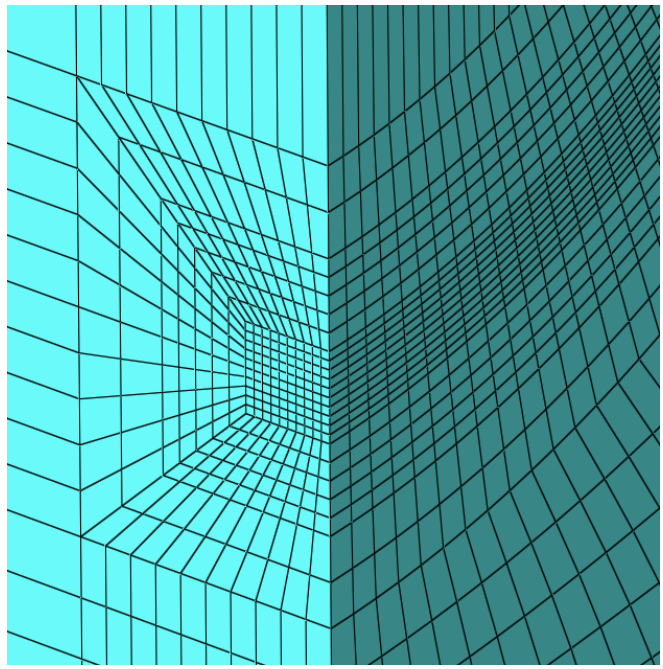

Figure 10: Close up picture of focused mesh in the crack area

4.3.1 Boundary conditions

In order to accieve results that are physically correct, the appropriate boundary conditions (BCs) must be assigned to the model. The BCs are shown in Fig. 11, where explainations also are included. However, a more thorough explaination will be given here. As the coordinate system defines the x-, y-, and z directions, the corresponding degrees of freedom (DOFs) are U1, U2 and U3 for translation and UR1, UR2 and UR3 for rotations. E.g. U1=1 means a translation of 1 unit in the x direction, and U2=1 means a rotation of 1 unit around the y axis.

BC1 and BC3 are assigned to the crack ligament and crack surface respectively. These surfaces are in the same plane. Still, separate BCs were assigned, so that BC3 could be released to simulate a crack being created after the welding residual stresses has been introduced. BC2 is assigned to symmetry plane which is mid width of the plate. BC4 is assigned in order to simulate an external load. Given the gross section of the plate, global yield will occur at U1 $\approx$ 0,4 mm. I.e. the value U1 = 0,6 mm is $\sim$1,5 times the displacement needed to cause yield. This,

along with minimum increment length, is carefully chosen with respect to the relevancy and accuracy of the results. BC5 is assigned to only one node, in the mid far corner. This is assigned in order to hinder a rigid body movement which can cause the solution to diverge rather than converge. BC6 is assigned to the rigid wall, shown in Fig. 12, in ordet to restrain any movement. Abaqus allows for introducing BCs stepwise. The sequence in which the BCs are assigned will be presented later.

4.3.2 Contact problem

As mentioned, tensile residual stresses are often present on the surface and compressive in the middle of a plate. As BC3 is released, there might be both tensile and compressive stresses on the crack surface. Compressive stresses might cause a negative nodal displacement, i.e. a negative CTOD. However, this is not physically possible as the opposing crack surface will hinder this displacement. To deal with this issue, a wall consisting of rigid shell elements was modeled as shown in 12. The wall was constrained so that is was coincident with the crack surface and ligament, and $W/2$ was always the same as one the model. I.e. 600 mm on all models. Contact was then assigned between this surface and the crack surface, where the rigid wall was the master surface and the rack surface the slave surface. "Node to surface" contact was then assigned, meaning that the nodes on the slave surface is not able to cross the rigid shell elements on the master surface. The contact properties that were assigned were "Hard contact" and frictionless parallel behavior. Assigning these properties, the model is very close to pysical correctness. Interactions must be assigned for each set of interacting surfaces. Only the mentioned interaction was assigned, named Int1.

4.3.3 Predefined fields

As mentioned, changing temperature was used to induce eigenstrain and create residual stresses in the weld zone. In Abaqus, this is done by assigning "Predefined Fields" (PFs). Two fields were created, PF1 and PF2, with temperatures 20°C and 21°C respectively.

4.3.4 Steps

As mentioned, loads, BCs and PFs can be applied stepwise in Abaqus, in order to achieve the preferred sequence. Each step has a duration of 1 unit, i.e. second, minute, or other unit. Note that time in Abaqus is unitless. Further, each step consists of one or more increment. The number of increments for each step can either be chosen automatically by Abaqus or defined by the user. If increment length is chosen by Abaqus, the user must define a maximum- and minimum

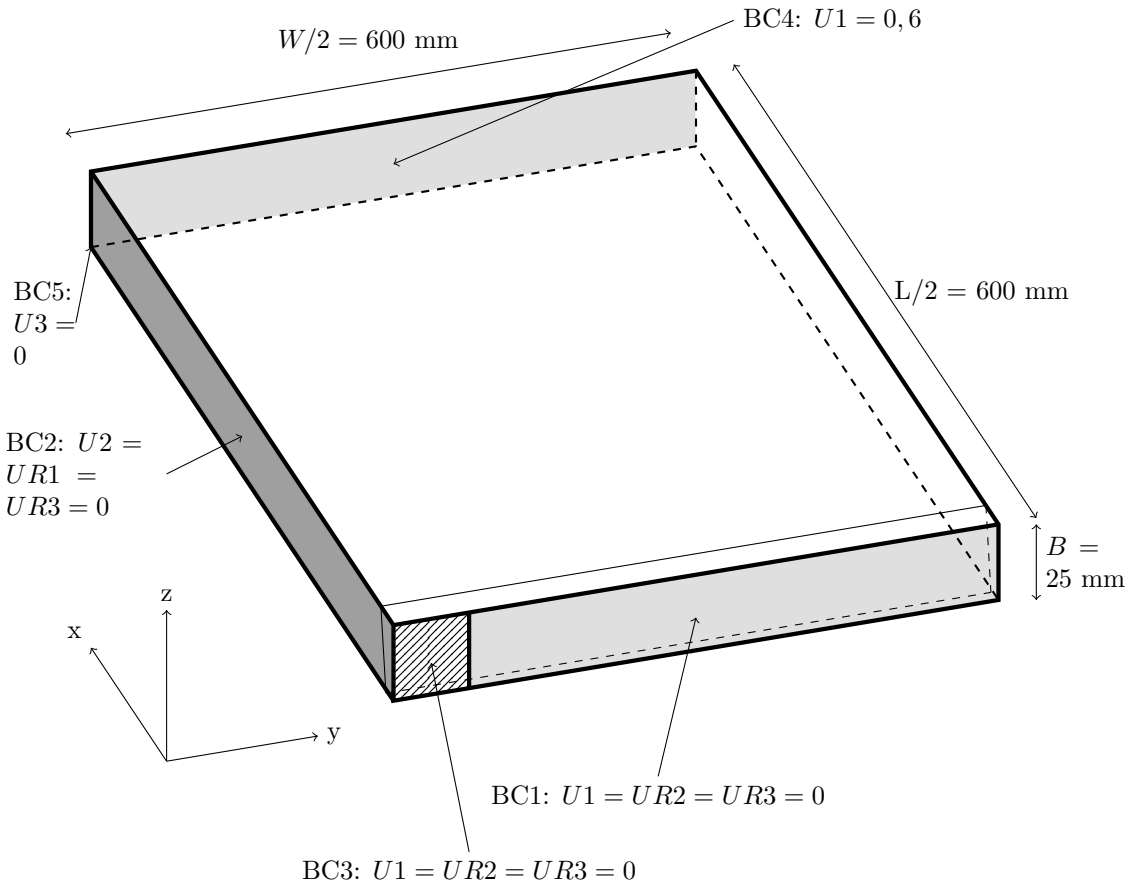

Figure 11: Sketch of model 2

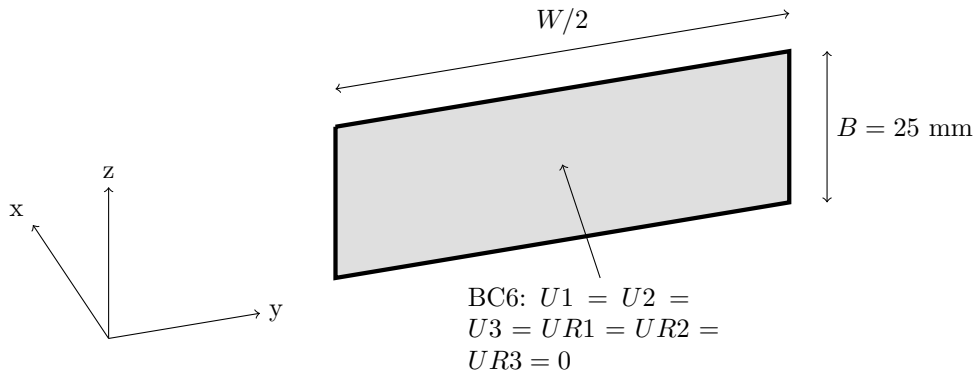

Figure 12: Sketch of rigid body

value. In this work, accurate results were needed for step 3, but not for step 1 and 2. As the desire was to plot the crack driving force, CTOD vs load, the maximum increment length was set as 0,05, meaning a minimum number of 20 increments for step 3. This way, a path can be plotted in the FAD and the critical point determined accurately for simulation. For step 1 and 2 accurate results were not necessary. Hence, the maximum increment length was set to 1. This was done in order to reduce the amount of data that was written. The minimum increment length was set to 10^{-5} for all steps as deafult by Abaqus.

4.3.5 Output requests

Before running a simulation in Abaqus, requsts must be made on what data that is written during the simulation. However, there are some preselected defaults requsts. So-called "Field -" and "History Output Requsts" can be made. The field output allows to user to plot color plots in the vizualization module. E.g. a color plot of Mises- or axial stress can be plotted across the entire model at chosen time step and increment.

Displacement in the x-direction of the node closest to the crack tip, i.e. U1, was requested in history output in the analysesm shown in Fig. 13. In this work, the distribution of residual stresses give tensile stresses in the surface and compressive stresses around the mid thickness. Thus, CTOD was taken at two different points for the surface cracks, i.e. at the deepest point, $\theta = \pi/2$ and the point where the crack front intersects the surface, $\theta = 0$. Taking CTOD from these two points cover both the point where the contribution from external loading is greatest, $\theta = \pi/2$ and the point where contribution for residual stresses

is greatest, $\theta = 0$. The nodal displacement was multiplied by 2 when CTOD was defined, due to symmetry. In addition the reaction force in the x-direction, i.e. RF1, of all nodes on to opposite surface was requested. These were summed up and divided by the cross section in order to detemine the nominal stress. When these two values are obtained for each increment, the fracture- and load ratio can be plotted in a FAD for each increment of step 3.

For fracutre mechanics analyses according to e.g. BS 7910 the nominal stress in required. In this work, the nominal stress in defined as the total forces in x-direction of the tension surface divided by the gross section. The "tension surface" is the surface where BC4 is working. This is shown in Eq. (27) and Eq. (28) where "all" means all nodes affected by BC4.

$$F = \sum_{all} RF1 \tag{27}$$

$$\sigma_{nom} = \frac{F}{A} = \frac{F}{B * W} \tag{28}$$

4.3.6 Sequence of loading

In the load module in Abaqus, the sequence of which the loads, BCs and PFs are applied is defined. In addition, the same can be done for interactions in the interaction module. Table 1 shows the sequence in which the BCs, PFs and interactions are applied and deactivated. This sequence of loading simulates a crack being created after the welding residual stresses are introduced. In practice, this means e.g. a fatigue crack that has occured in the service time of a structure, hereafter called cold cracks.

In practice, cracks can also be created during welding, herafter hot cracks. To illustrate the differents effect of hot and cold cracks on fracture behavior, a number of extra simulations were run where BC3 never was active. The simulations were on model 3 with shallow cracks, $a = 5$ mm. The full sequence of loading is shown in Table 2

As this work focuses on the effect of residual stresses on fracture resistance, it is necessary to compare the results of a crack in a RS field, with a reference model, without residual stresses. This way, the results can be compared and the effect of residual stresses clearly shown. Hence, another simulation was run for each crack length, where the sequence of loading is given in Table 3. The reference model is the exact same as model 1, 2 or 3, i.e. geometry and mesh is the exact

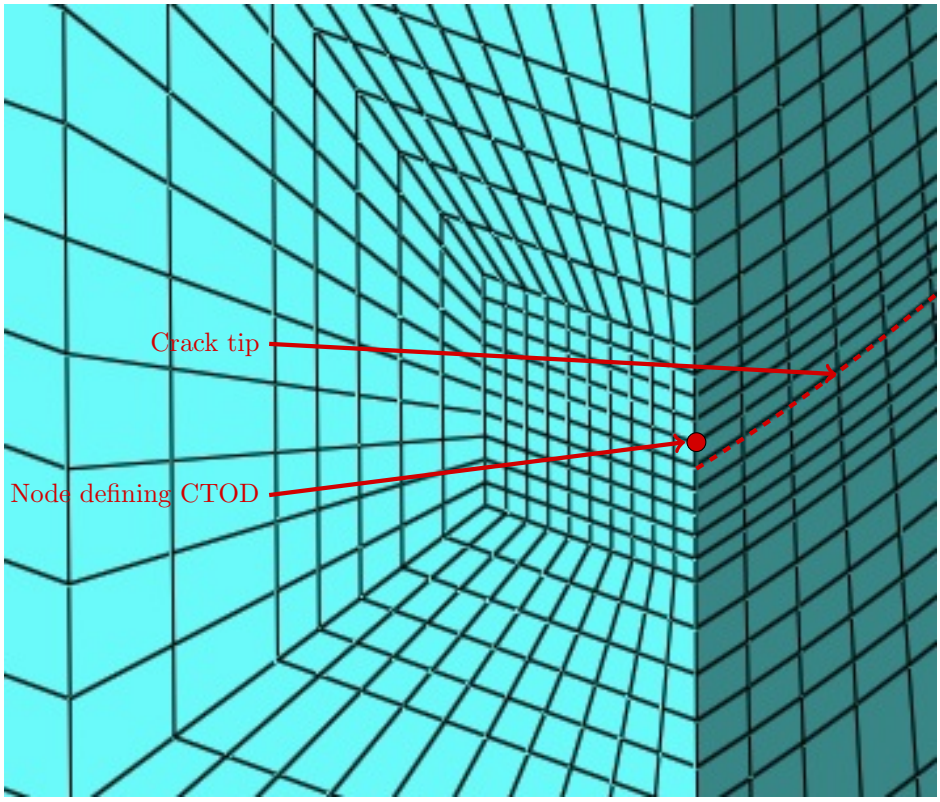

Figure 13: Node defining CTOD

Load name	Initial	Step 1	Step 2	Step 3
BC1	Active	Active	Active	Active
BC2	Active	Active	Active	Active
BC3	Active	Active	Deactived	Inactive
BC4	Inactive	Inactive	Inactive	Active
BC5	Active	Active	Active	Active
BC6	Active	Active	Active	Active
PF1	Active	Deactivated	Inactive	Inactive
PF2	Inactive	Activated	Inactive	Inactive
Int1	Inactive	Inactive	Activated	Active

Table 1: Sequence of loading for cold crack in RS field

Load name	Initial	Step 1	Step 2	Step 3
BC1	Active	Active	Active	Active
BC2	Active	Active	Active	Active
BC3	Inactive	Inactive	Inactive	Inactive
BC4	Inactive	Inactive	Inactive	Active
BC5	Active	Active	Active	Active
BC6	Active	Active	Active	Active
PF1	Active	Deactivated	Inactive	Inactive
PF2	Inactive	Activated	Inactive	Inactive
Int1	Inactive	Inactive	Activated	Active

Table 2: Sequence of loading for hot crack in RS field

Load name	Initial	Step 1	Step 2	Step 3
BC1	Active	Active	Active	Active
BC2	Active	Active	Active	Active
BC3	Inactive	Inactive	Inactive	Inactive
BC4	Inactive	Inactive	Inactive	Active
BC5	Active	Active	Active	Active
BC6	Active	Active	Active	Active
PF1	Inactive	Inactive	Inactive	Inactive
PF2	Inactive	Inactive	Inactive	Inactive
Int1	Inactive	Inactive	Activated	Active

Table 3: Sequence of loading for reference models

same. Both PFs though, are always inactive through all steps. The same output requests were made here.

5 Results

In this section the most relevant results as well as the post-treatment of the results and how the data was interpreted is presented.

5.1 Implementing results in FAD

As stated above, a FAD assesses the possibility of both brittle and ductile fracture. According to LEFM theory, the stress intensity factor is proportional to the applied stress, i.e. plotting K_r vs L_r will result in a linear plot. However, this is only valid within the limits of LEFM. In this work, the fracture ratio, $\sqrt{\delta_r}$, and load ratio, L_r, are calculated separately from FEM. As plasticity at the crack tip occurs at significantly lower load than global yielding, the load is not linear if plotted directly into the FAD. However, the assessment line takes account for the increasing gradient of the effective crack driving force as load increase. Hence, the fracture ratio, $\sqrt{\delta_r}$, measured for FEM is multiplied with the assessment line given by Eq. (12), in order to be comparable with load paths according to BS 7910.

The load according to BS 7910 is linear, with gradient according to LEFM. The contribution from residual stresses is added to the fracture ratio, which alternatively can be set equal to the lower of Eq. (15) and Eq. (16). This results in a linear plot where the gradient becomes lower at stresses equal to 0,4 times the flow strength, σ_f. However, looking at Fig. 14, and assuming this is the real disutribution of residual stresses, it can be seen that setting the residual stresses equal to the yield strength is overly conservative.

BS 7910 also allows use of the real distribution of residual stresses, if known. If results from FEM were to be comparable to implementation of residual stresses according to BS 7910, Fig. 14 is used as the real stress distribution. In this case the stress varies over the crack front. In the cases of through thickness cracks the contribution from external loading to crack driving force, $(Y\sigma)_p$, is equal over the crack front and the contribution from residual stresses, $(Y\sigma)_s$, is therefore equal to the highest residual stress through the thickness. In the cases of surface cracks with $a = c$ the contribution form external loading is approximately equal over the crack front. The contribution from residual stresses however if greatest at the surface. Hence, the point where the crack front meets the surface was used in the assessments. In cases of surface cracks with $a < c$, the contribution to crack driving force from external loading is greatest at the deepest point. However, the residual stresses were highest at the surface. Therefore, two loading paths

was plotted, at the surface and at the deepest point of the crack. I.e. $\theta = 0$ and $\theta = \pi/2$ in Fig 6.

5.2 Results from FEM

The fracture ratio used in the work is $\sqrt{\delta_r}$, is given in Eq. (4), where δ_{mat} is set to 0,1 mm. This is the lowest required CTOD toughness in Arctic materials KMB project guideline[10], and is the requirement for elastic design, i.e. for utilisation of up to 80% of the material yield strength. The fracture ratio was calculated for each increment of step 3. This was done, extracting displacement of the node clossest to the crack tip from the result file, in tabular format and plotting it into Microsoft Excel. This was done for each simulation, i.e. each crack in either model 1, 2 or 3, and compared to the corresponding reference model. The membrane stress, P_m, was calculated by dividing the reaction force, RF1, with the gross section of the model. The bending stress, P_b, was zero due to only membrane loading. L_r was calculated according to Eq. (7) to Eq. (11), for each increment. Hence, one point on the FAD could be plotted for each increment in step 3.

5.2.1 Residual stress field induced by eigenstrain

As mentioned, residual stresses was introduced in the FEM model using the eigenstrain method. Using thermal expansion, the weld section had en eigenstrain of $\alpha = 0,003$, i.e. the volume of this section was increased by 0,003 times the original volume. The base section was assigned with $\alpha = 0$, meaning that this section only restrain the increase in volume of the weld section. This strain is what create the residual stresses in FEM. It can be seen from Fig. 14 that there are tensile stresses in the surface, while there are compressive in the middle. Fig. 14 is extracted from Abaqus at the end of step 1 in the intersection of both symmetry planes, i.e. where the deepest point of the surface cracks are located. All points in the distribution are shown in Annex C. Fig. 15 shows the distribution of residual stresses on both surfaces of the plate along the crack ligament, i.e. the same plane as all crack were located. All cracks are located so that the center of the crack is at $\frac{d}{W/2} = 0$. Hence, the stress field through the thickness is assumed equal over the width of the plate, i.e. equal in the areas where the cracks investigated were located.

BS 7910 suggests a number of different distributions of residual stresses for different geometries[11, Annex Q]. For butt-welded plates Fig. 14 is within the suggested area. It must be mentioned, however, that the range of the suggested area is vast, i.e. Stesses at the surface between $\sim -0,6 * \sigma_Y$ and $\sim \sigma_Y$. Below the

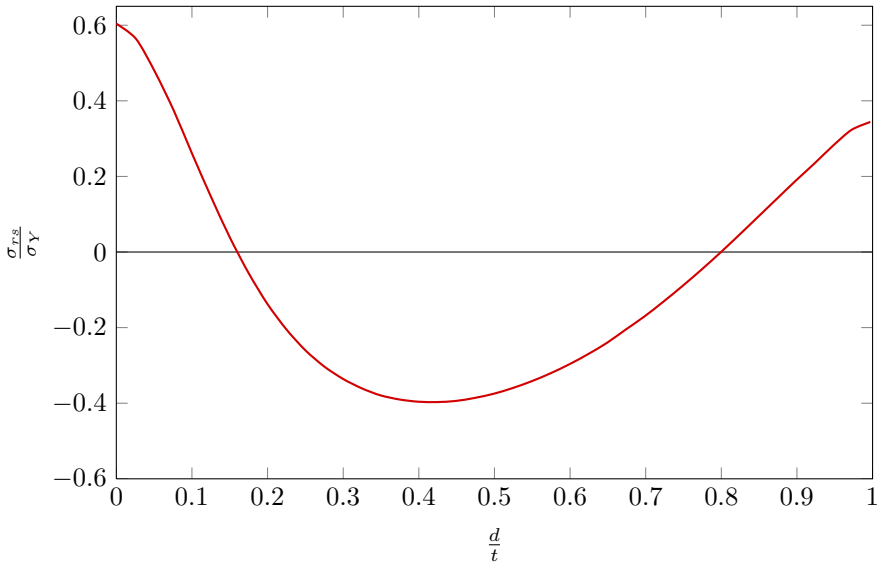

Figure 14: RS field through thickness, $\alpha = 0,003$, $\sigma_Y = 420$ MPa, $t = 25$ mm

surface, the suggested distribution is more consistant and range from $\sim -0,6 * \sigma_Y$ to $\sim -0,4 * \sigma_Y$.

5.2.2 Load and fracture ratio according to BS 7910

According to BS 7910 the fracture ratio is calculated from the reference stress, σ_{ref}. Recall Eq. (13) to Eq. (16) and Eq. (19) to Eq. (22). Where P_m and Q_m are the membrane stresses from external load and residual stresses. P_b and Q_b are bending stresses from external load and residual stresses which are set to zero here duo to the loading only being axial. Note that $(Y\sigma)_p$ in Eq. (19) is solely defined by geometry of the plate and crack, i.e. the right side of the equation depend on the geometry, but is not presented here due to complexity.

In order to plot a loading path in a FAD according to BS 7910, P_m was set equal to the gross section stress on the reference model, i.e. the sum of the reaction force, RF1, of all nodes on the tension surface divided by the gross area of the plate. The residual stresses were assumed to be equal to the yield strength, i.e. 420 MPa, or with relaxation. Note that the yield strength is equal for both the base- and weld material in the FEM analyses. This is according to BS 7910 which states that the lowest of the base and weld material yield strength shall be

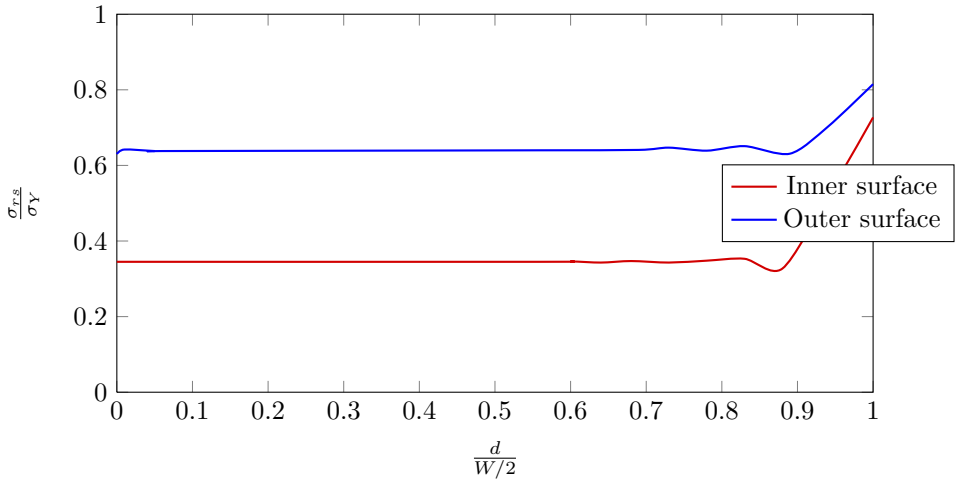

Figure 15: RS field along crack ligament, $\alpha = 0,003$, $\sigma_Y = 420$ MPa, $t = 25$ mm

used. As BS 7910 also allows the real distribution of residual stresses to be used if known, this was also done.

5.2.3 Level 2B FAD assessment line

Given the above sections, the load paths according to FEM for model 1, 2 and 3 with the reference models and according to BS 7910 can be plotted in a FAD, shown in Fig. 4. As stated, the level 2B assessment line is used, taking material properties into account. The assessment line is given by Eq. (12), where ε_{ref} is given by Eq. (25). Note that ε_{ref} and L_r are uniquely ralated, i.e. the assessment line is a function of L_r.

5.2.4 Loading paths

The loading paths from FEM were plotted using Eq. (4) and Eq. (7). When the loading path was plotted according to BS 7910, the same formulae, in addition to Eq. (5) that was used for converting applied K_I to applied δ_I, was used. K_I was first calculated according to Eq. (13) to Eq. (16) and Eq. (19) to Eq. (22). For results from FEM, loading paths were plotted for each crack length. Loading paths were also plotted for all corresponding reference solutions. According to BS 7910, the path were plotted with both the option of $Q_m = \sigma_Y$ with relaxation and Q_m taken from the real stress distribution shown in Fig. 14. The main focus was on assessments where Q_m is taken from Fig. 14.

5.2.5 Effect of residual stresses

Showing the loading path in a FAD, however, does not show the effect of residual stresses clearly. Hence, subtracting the fracture ratio from each referance model form the fracture ratio from the solution with residual stresses will result in the difference in fracture ratio caused by residual stresses. This was done according to Eq. (29), where $\sqrt{\delta_r}$ and $\sqrt{\delta_r}_{Refsolution}$ are fracture ratios from solutions with residual stresses and corresponding reference solution, and $\Delta\sqrt{\delta_r}$ denotes the difference in fracture ratio caused by residual stresses.

$$\Delta\sqrt{\delta_r} = \sqrt{\delta_r} - \sqrt{\delta_r}_{Refsolution} \tag{29}$$

Further, it is relevant to investigate the effect of residual stresses compared to the frature ratio for the reference solution. This was done according to Eq. (30), where the effect of residual stresses is named R in this work. R is a dimensionless parameter, developed during this work and denotes the effect of residual stresses. Determining the R according to Eq. (29) and Eq. (30) was done both for results from FEM and according to BS 7910. Reference solutions were calculated both for FEM and according to BS 7910.

$$R = \frac{\Delta\sqrt{\delta_r}}{\sqrt{\delta_r}_{Refsolution}} = \frac{\sqrt{\delta_r} - \sqrt{\delta_r}_{Refsolution}}{\sqrt{\delta_r}_{Refsolution}} \tag{30}$$

It can be seen that the fracture ratio alternatively can be expressed as a function of the fracture ratio for the referenace solution and R, which vary with L_r.

$$K_r \text{ or } \sqrt{\delta_r} = \sqrt{\frac{\delta_I}{\delta_{mat}}} = \sqrt{\delta_r}_{Refsolution} * (1 + R) \tag{31}$$

5.3 Model 1 - surface cracks, $a = c$

In this section, the results from model 1 are presented. Looking at Fig. 14, it can be seen that the highest stresses are at the surface, i.e. the contribution to crack driving force is highest here. Looking at Eq. (23) to Eq. (24) the driving force for a circular crack is approximately equal over the crack front, assuming no residual stresses. This means that the point with the greatest driving force is at the plate surface. Hence, only results from $\theta = 0$ are shown.

5.3.1 Summary of results

Figs. 17 to 20 show examples of plots that were made based on results from FEM and compared to a fractue assessment according to BS 7910. It can be

seen that assuming the residual stresses to be equal to the yield strength is not more conservative than taking the residual stress from the real distribution for $a = 10$ mm, at the point where the load path crosses the assessment line, hereafter called the critical point. Such assessment consideres a crack with depth and length $a = c = 20$ mm unsafe at zero load. Note that the first points on the load path according to BS 7910 where the residual stress is equal to the yield strength is not included as the detailed approach for determining ρ is needed. However, assessments where the residual stresses are equal to yield is not the focus as the resiudal stresses in the FEM models are significantly lower. Using this the distribution shown in Fig. 14 has been the main focus. The maximum stress from this distribution of residual stress is $\sim 0,6 * \sigma_Y$. Fig. 14 is the real distribution and the stress at the surface is the highest, i.e. $Q_m = 253,6$ MPa. Using the distribution of, the relaxation according to Eq. (15) is not allowed. However, there is a relaxation when using the real distribution, which is included in ρ in Eq. (4). The correction factor ρ is $\sim 0,7$ at $L_r = 0$ starts decreasing significantly at $L_r \approx 0,8$ and is zero at $L_r \approx 0,9 - 1,2$ for the cases presented here. Note that ρ is only used when calculating $\sqrt{\delta_r}$ according to BS 7910, i.e. not for results from FEM.

It must be noted that X in Eq. (5), it is assumed that $X = 1,5$ in this work. Recall, X is, according to BS 7910, usually in the range 1 to 2, where 1 is conservative. X is very significant for the gradient of the loading paths plotted according to BS 7910. It is stated in BS 7910 that X can be determined from elastic-plastic analyses, or conservatively assumed 1. The gradient of the curves according to BS 7910 and FEM are often approximately equal, using $X = 1,5$. Thus, the assumed value of $X = 1,5$ is considered neither conservative or underconservative, but rather reasonable.

5.4 Model 2 - through thickness cracks

In this section, the results form model 2 will be briefly presented, along with observations that are considered interesting. The load path is plotted using two different options in BS 7910 and compares to results from FEM.

5.4.1 Summary of results

Fig. 21 does not show the load path when the residual stress at the crack tip is assumed equal to the yield strength. According to such assessment, the crack is considered unsafe at zero load and is outside the diagram shown. However, using the real distribution of residual stresses, Q_m is significanly lower. In this case the contribution from residual stress to the crack driving force is set equal to the maximum stress for the distribution over the thickness, i.e. $Q_m = 253,6$ MPa.

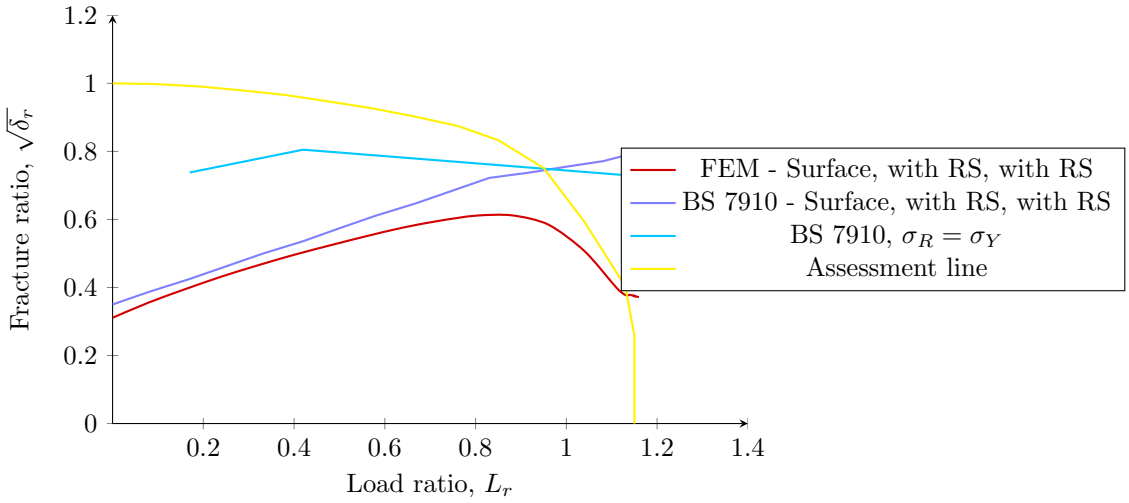

Figure 16: Level 2B FAD for model 1 with crack depth, $a = 10$ mm, surface point, $\theta = 0$

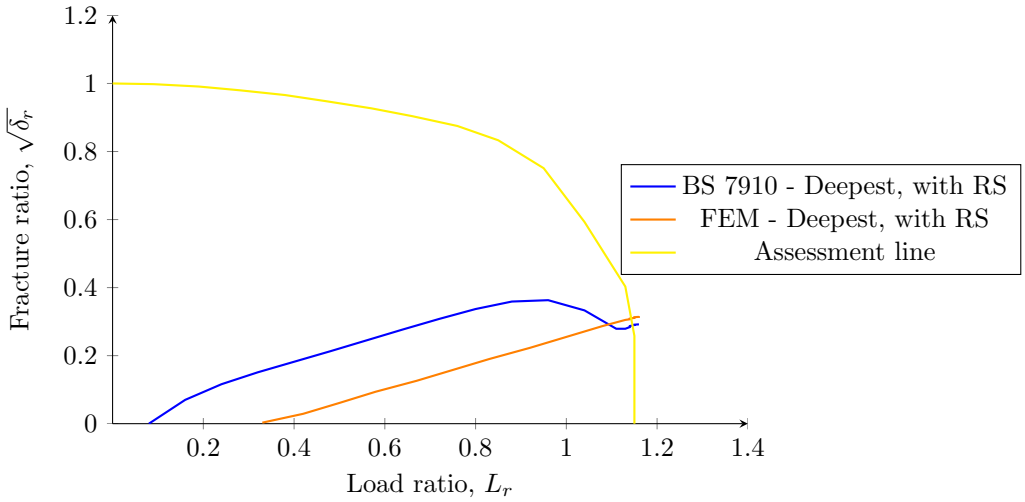

Figure 17: Level 2B FAD for model 1 with crack depth, $a = 10$ mm, deepest point, $\theta = \pi/2$

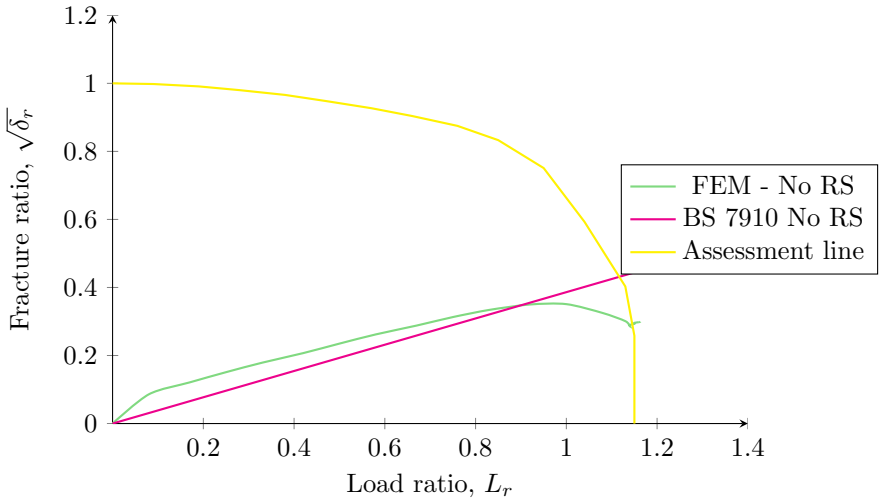

Figure 18: Level 2B FAD for reference model 1 with crack depth, $a = 10$ mm, surface point, $\theta = 0$

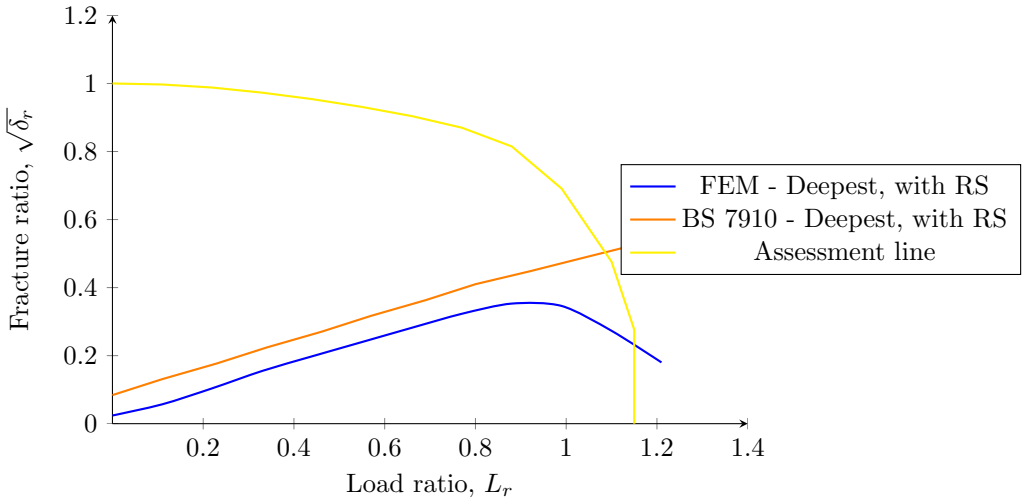

Figure 19: Level 2B FAD for model 1 with crack depth, $a = 20$ mm, deepest point, $\theta = \pi/2$

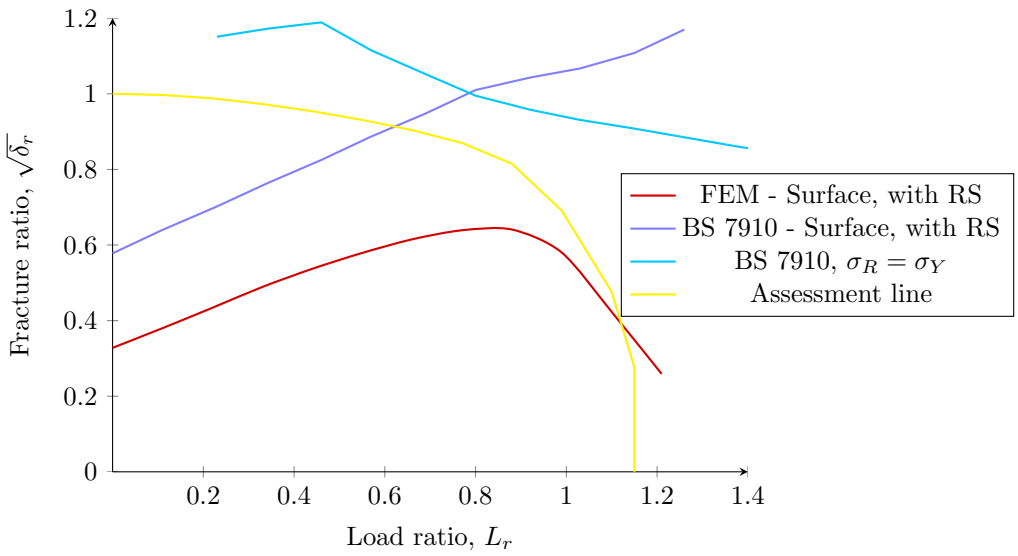

Figure 20: Level 2B FAD for model 1 with crack depth, $a = 20$ mm, surface point, $\theta = 0$

This is the same point as where the CTOD is measured from. The load path from FEM is plotted as shown in in Fig. 21 with both load- and fracture ratios taken directly from FEM. The corresponding fracture ratio was then calculated accroding to BS 7910 where i.e. $Q_m = 253,6$ MPa and plotted separately. It can be seen that when the load path is plotted according to this it is considered unsafe at significantly lower load than according to FEM.

It can be seen from Fig. 21 that both options according to BS 7910 are conservative. It must be noted that assuming the contribution from residual stresses to be equal to the material yield strength is not comparable to the distribution of residual stresses in FEM. The maximum stress from the distribution used in FEM was $\sim 0,6 * \sigma_Y$.

5.5 Model 3 - surface cracks, $a < c$

In this section, the results from simulations on model 3 will be presented. Results from model 1 with $a = c = 5$ mm are also included here, in order to discuss the effect of a/c ratio, keeping a constant. Looking at cracks where, $a < c$, the crack driving force will vary more significantly along the crack front

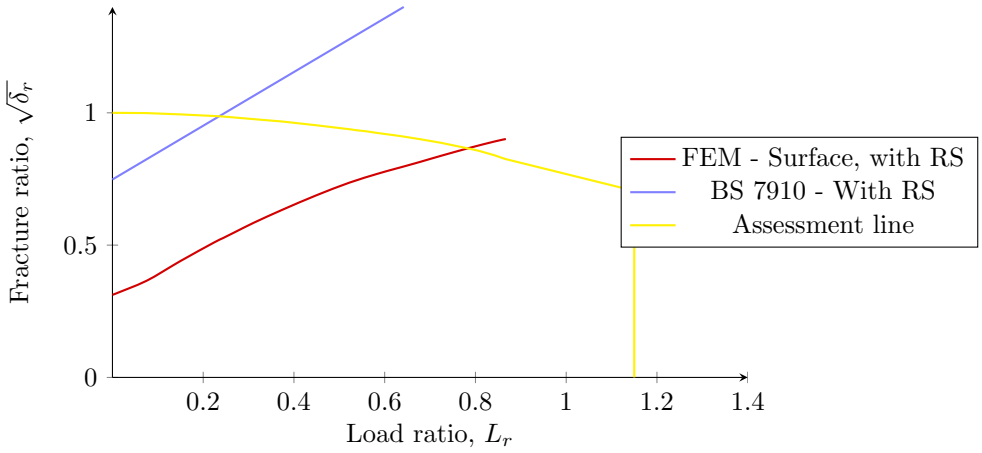

Figure 21: Level 2B FAD for model 2 with crack length, $a = 27,5$ mm

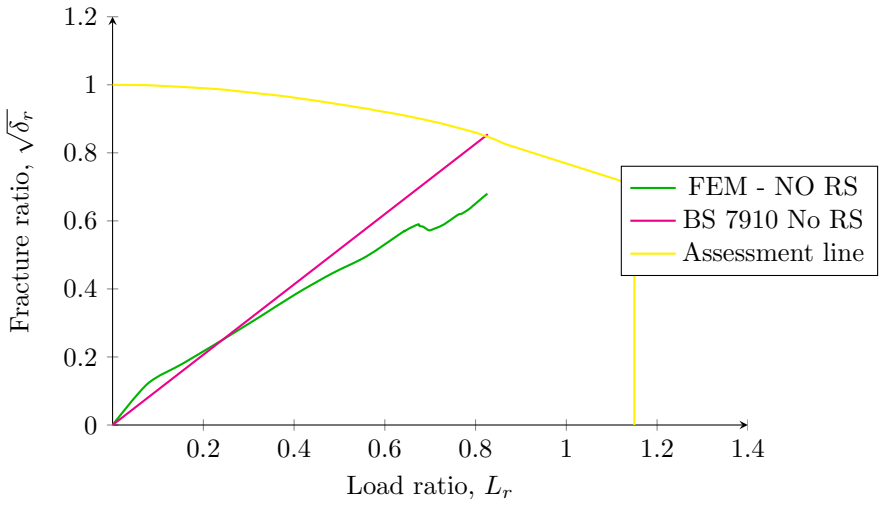

Figure 22: Level 2B FAD for model 2 with crack length, $a = 27,5$ mm

than in cases where $a = c$. Recall Fig. 6 and Eq. (23) to Eq. (24), it can be seen that in cases where $a < c$, the contribution from external load to crack driving force is greatest at the deepest point of the crack. I.e. $\theta = \pi/2$. However, looking at Fig. 14, it can be seen that the residual stresses are highest at the surface, i.e. $\theta = 0$. Note that assessments where the residual stress at the crack tip is assumed equal to the yield strength is not included here.

5.5.1 Summary of results

Figs. 23 to 25 show results plotted in FAD for the same crack, i.e. $a = 5$ mm, $2c = 30$ mm. At $L_R <\sim 0,8$ results from FEM and BS 7910 are very similar at the surface, $\theta = 0$. However, the relaxation at $L_r \geq\sim 0,8$ does not seem to be sufficient to correspond with the results from FEM. Note that the relaxation is inferred by ρ in Eq. (4), which is included in $\sqrt{\delta_r}$ according to BS 7910 but not FEM. It must be mentioned, however, that $\sqrt{\delta_r}$ for FEM is multiplied by the assessment line level 2B in order to be comparable with loading paths according to BS 7910. It is assumed that this is approximately, but not entirely accurate. In order to have a closer comparison results a level 3C assessment line can be used. However, this is not done is this work and is explained in the Discussion section.

When there are compressive residual stresses occuring at the crack tip BS 7910 dictates a negative crack driving force at zero load, which is not in agreement with results from FEM. This disagreement may by a result of significantly higher tensile stress in the surface, $\theta = 0$, than the compressive stress at the deepest point, $\theta = \pi/2$. As there are sompressive stress at the deepest point, $\rho = 0$ in Eq. (4) at all values of L_r. Thus, BS 7910 does not allow for any relaxation is cases where there are compressive residual stresses at the crack tip. This is not in agreement with FEM where a relaxation can be seen at $L_r >\sim 0,9$.

5.5.2 Hot cracks

Simulations were also run on model 3, simulation hot cracks. A hot crack is a crack that is present when the residual stresses are introduced. In FEM the sequence of loading for hot cracks simulations is shown in Tab. 2. Simulations were run on the same cracks for both hot and cold crack in order to get comparable results. It must be noted here that BS 7910 does not distinguisk between hot and cold cracks.

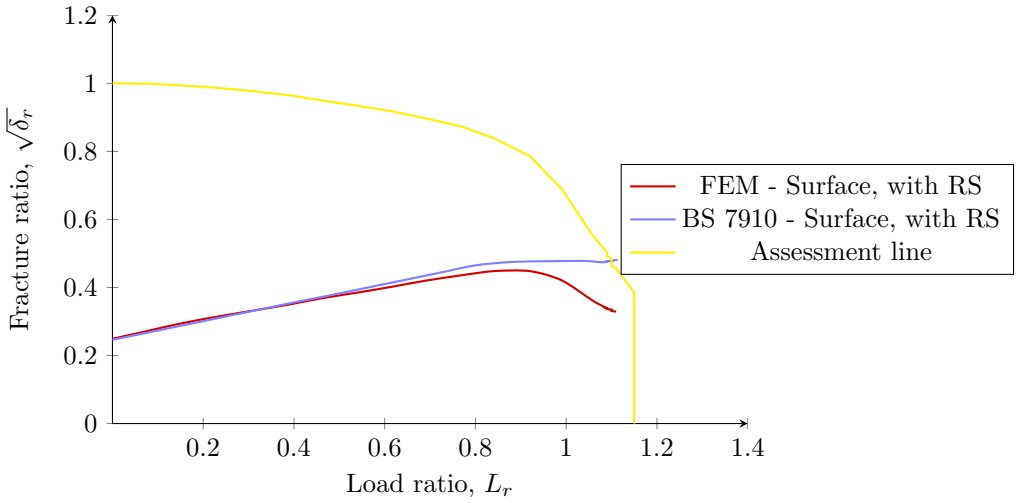

Figure 23: Level 2B FAD for model 3 with crack depth, $a = 5$ mm, crack length $2c = 30$ mm, surface point, $\theta = 0$

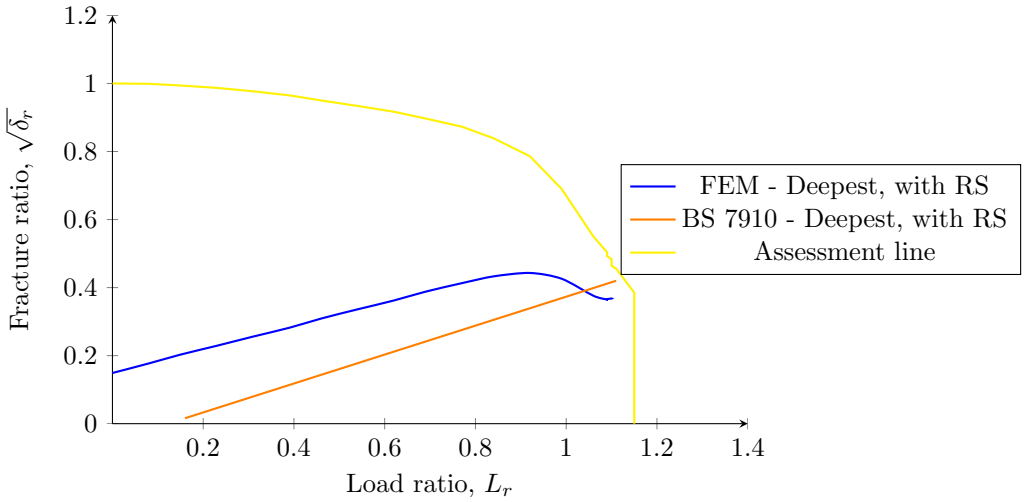

Figure 24: Level 2B FAD for model 3 with crack depth, $a = 5$ mm, crack length $2c = 30$ mm, deepest point, $\theta = \pi/2$

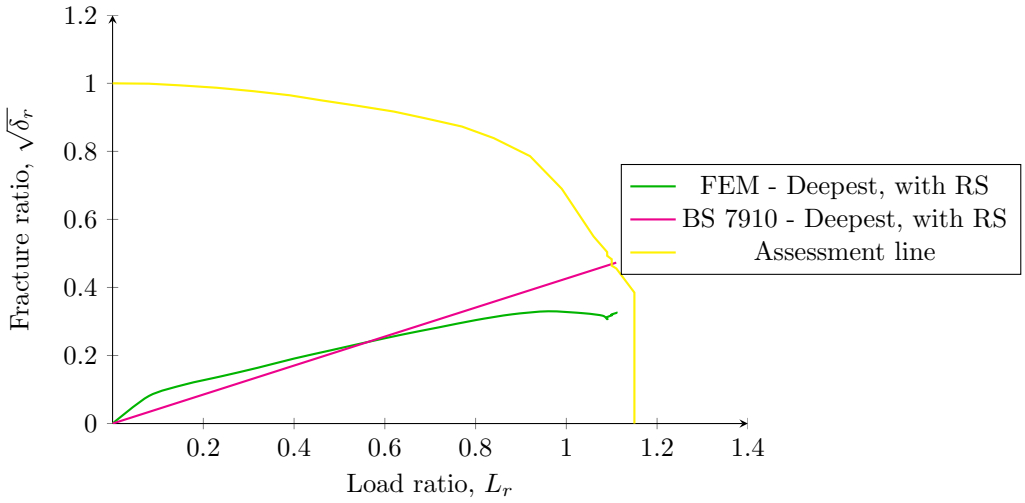

Figure 25: Level 2B FAD for reference model 3 with crack depth, $a = 5$ mm, crack length $2c = 30$ mm, deepest point, $\theta = \pi/2$

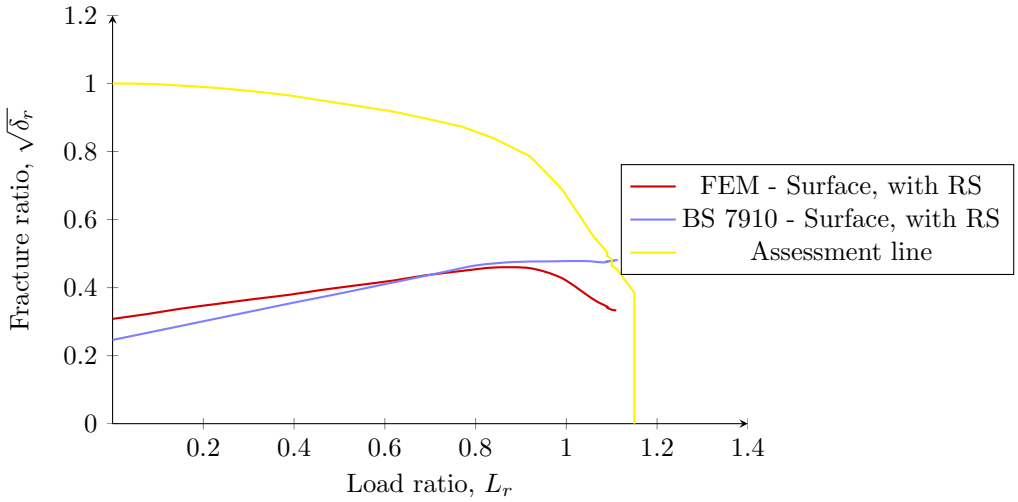

Figure 26: Level 2B FAD for model 3 with crack depth, $a = 5$ mm, crack length $2c = 30$ mm, surface point, $\theta = 0$, hot crack

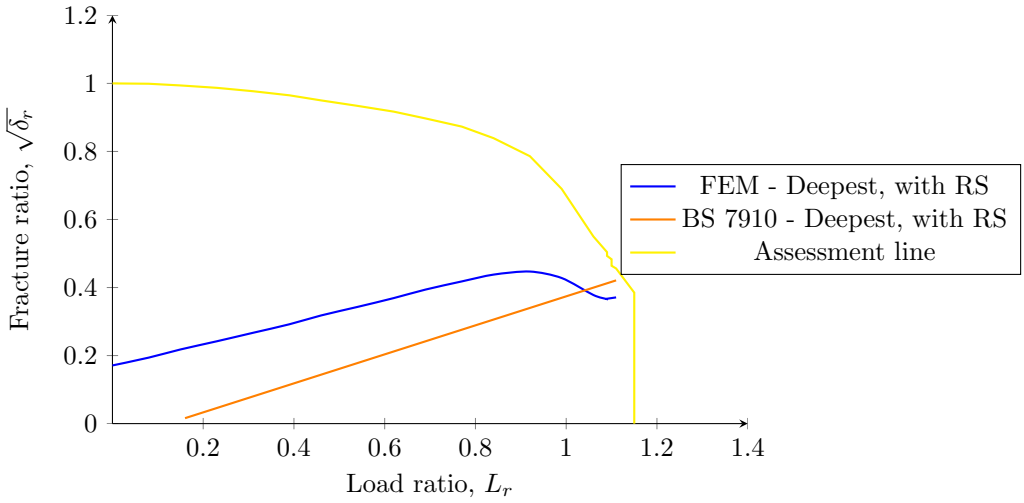

Figure 27: Level 2B FAD for model 3 with crack depth, $a = 5$ mm, crack length $2c = 30$ mm, deepest point, $\theta = \pi/2$, hot crack

6 Discussion

In this section, the effect of residual stresses, R, is determined for all cracks investigated. Conditions that affect R are also discussed, both according to FEM and BS 7910. The validity of the numerical set up and results will be disscused. The comparability between treatment of residual stresses in BS 7910 results from FEM will also be discussed. The aim is to point out any weaknesses with the approaches used in this work and aid further work on the subject.

6.1 Effect of residual stresses according to FEM and BS 7910

As mentioned, the effect of residual stresses in this work, denoted R, is computed according to Eq. (29) and Eq. (30). This was done both for results from FEM and BS 7910 in order to compare R as a function of L_r. Only cases were the residual stress at the crack tip is taken from Fig. 14 or Annex C is considered here, as the cases where the residual stress is assumed equal to the yield strength is not comparable with FEM. Comparison of R according to FEM and BS 7910 is discussed here. Note that the results from FEM are taken from simulations on cold cracks. The effect of hot cracks vs cold cracks is discussed later.

6.1.1 Model 1

The crack driving force in a plate with residual stresses according to FEM analyses and the corresponding solutions according to BS 7910 is shown in Figs. 17 to 18. The effect of residual stresses, R, is calculated according to Eq. (29) to Eq. (30). It can be seen that R is a function of L_r. Figs. 28 to 30 show R as a function of L_r for $a = c = 5$ mm, $a = c = 10$ mm and $a = c = 20$ mm respectively. Note that all solutions with corresponding reference solutions were either from FEM or BS 7910, i.e. no result from FEM has a reference solution according to BS 7910 or vice versa.

It can be seen that the effect of residual stresses according to FEM decrease as L_r increase for all crack depths. Likewise for results according to BS 7910. It was postulated earlier that BS 7910 overestimates the effect of residual stresses. However, it is shown that this is not universally true. As the crack size increase, while $a/c = 1$ is kept constant, it can be seen from Figs. 28 to 30 that BS 7910 eventually overestimates the effect of residual stresses. An explaination for this might lie in the distribution of residual stresses, shown in Fig 14. As crack depth increase, the residual stress at the deepest point of the crack decrease. Thus, the average stress on the crack surface becomes lower. BS 7910 however, dictates that the residual stress at the assessment point is used as the contribution to crack

driving force from residual stresses. The assessment point here is the point where the crack intersects the surface, i.e. where the residual stresses and resulting crack driving force are greatest.

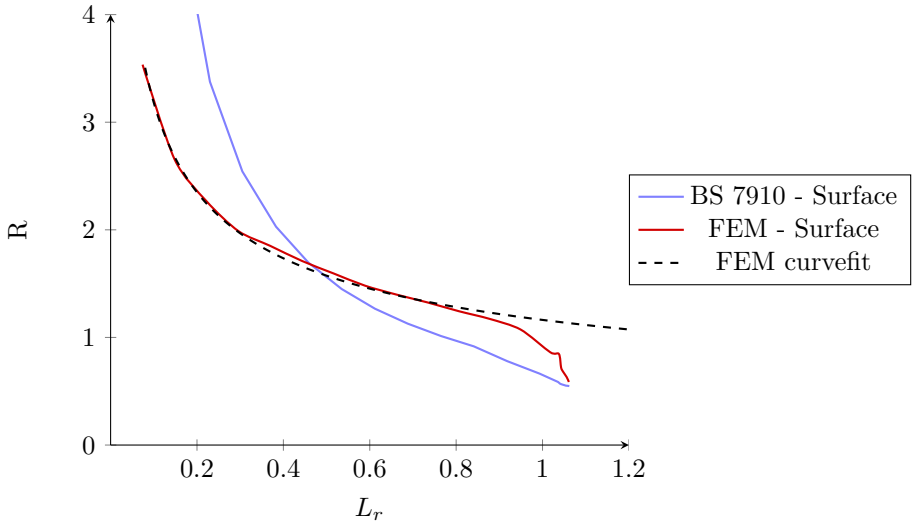

Figure 28: Effect of residual stresses in level 2B FAD for model 1 with crack depth, $a = 5$ mm, crack length $2c = 10$ mm, surface $\theta = 0$

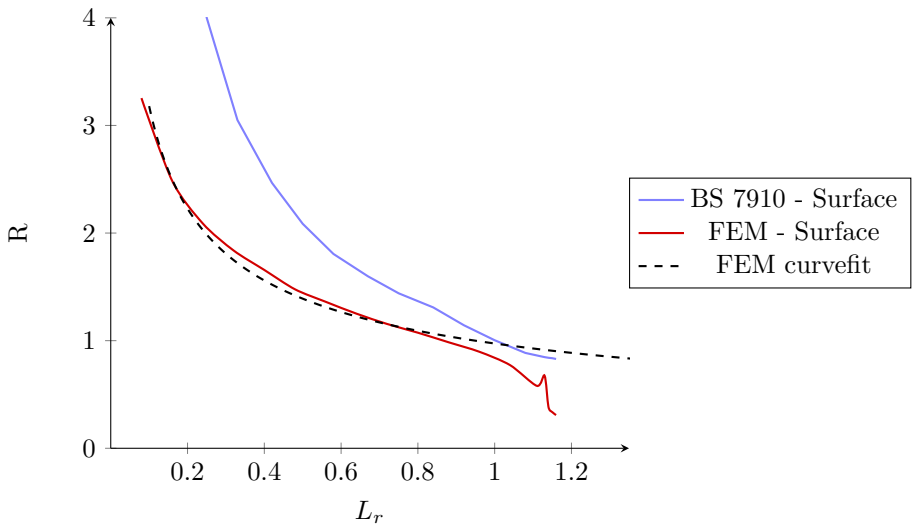

Figure 29: Effect of residual stresses in level 2B FAD for model 1 with crack, $a = c = 10$ mm, surface $\theta = 0$

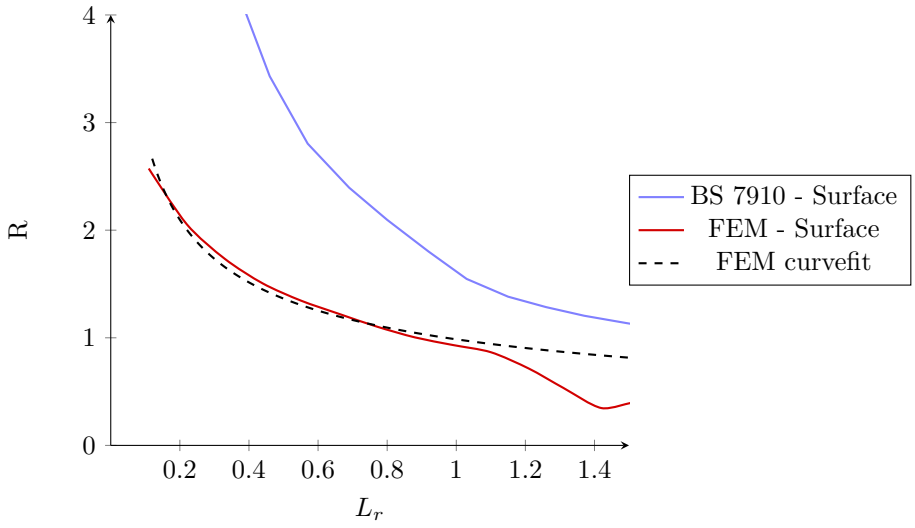

Figure 30: Effect of residual stresses in level 2B FAD for model 1 with crack, $a = c = 20$ mm, surface $\theta = 0$

6.1.2 Model 2

Fig. 31 shows the effect of residual stresses for a through thickness crack with $a = 27,5$ mm, computed according to Eq. (29) to Eq. (30). Both results according FEM and BS 7910 are shown.

According to BS 7910, the effect of residual stresses is overestimated significantly, compared to FEM. As noted in Section 6.1.1 the residual stresses vary over the crack front. In the case of through thickness cracks Fig. 14 is the approximate distribution of residual stresses over the crack front. As the stress field in Fig. 14 is a self-equilibrating field the average stress is zero over the crack front. According to BS 7910 however, the contribution from residual stresses are taken from the point where the residual stresses are greatest, i.e. $\sim 0,6 * \sigma_Y$. This assumption is likely the reason for the conservatism according to BS 7910.

It can also be seen that the effect according to FEM is inconsistent, with sudden jumps. A cause of this might be that the Load ratio, L_r, for each increment was not coincident for the simulation with residual stresses and the reference solution. Therefore, linear interpolation was used. Other factors may also have an impact, which will be more thoroughly presented in the later. It can also be seen from Fig. 31 that curvefitting does not fit as well as for surface cracks. However, Fig. 31 indicates that BS 7910 overestimates the effect of residual stresses.

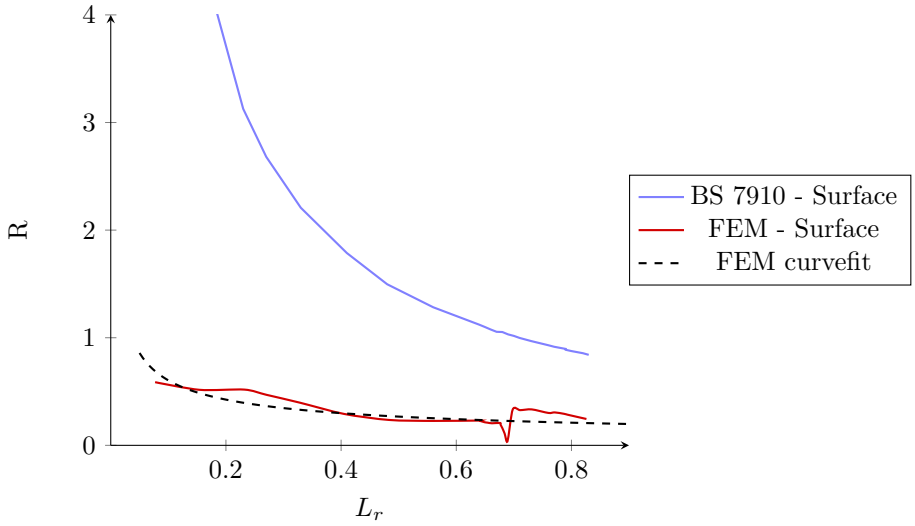

Figure 31: Effect of residual stresses in level 2B FAD for model 2 with crack, $a = 27,5$ mm, outer surface

6.1.3 Model 3

Figs. 32 to 37 shows the effect of residual stresses according to Eq. (30) as a function of L_r. Results according to both FEM and BS 7910 are presented. Note that, results for $a = c = 5$ mm is also presented with results from model 1, but is included here in order to prove a better basis for discussion of the the effect of the a/c ratio. Assessments at both the surface and deepest point are relevant as the residual stresses are greatest at the surface, while the contribution to crack drving force from external loading is greastest at the deepest point.

At the surface point, $\theta = 0$, the same trend as for cracks with $a = c$ can be seen, i.e. that the effect of residual stresses descrase as load increase, shown in Figs. 32 to 34. This occurs throughout the results without exeptions, both according to BS 7910 and FEM. As with model 1, BS 7910 underestimate the effect of residual stresses for small cracks, but overestimates for larger cracks, for $\theta = 0$. Note that larger in this context means that the crack length, c, is greater, as a is kept constant. For model 1 however, the average stress, from the residual stress distribution, over the crack surface decrease as the crack size increase. For model 3 this effect is the opposite, the averagve stress at the surface will increase as c increase. This can be seen from Fig. 14. A greater share of the crack surface is close to the surface of the plate, where the residual stresses are greatest. Still, the same trend as for model 1 is seen, i.e. that the BS 7910 becomes increasingly conservative as crack size increase for $\theta = 0$.

Is also relevant to assess the deepest point of the crack, $\theta = \pi/2$. It can be seen from Figs 35 to 37 that the residual stresses, according to FEM, contribute to crack driving force, i.e. R is positive, even tough the residual stresses at this assessment point are compressive. This might be caused by the high positive residual stresses on the crack surface close to the plate surface. BS 7910 however, dictates that the residual stresses at this assessment point, give a negative contribution to crack driving force, i.e. R is negative for all values of L_r. BS 7910 is not in agreement with FEM at this assessment point. As the average residual stress is positive over the crack surface intuition suggests that the residual stresses contribute to crack driving force, i.e. R is positive. In practice however, knowledge about the distribution of residual stresses may be not available. Hence, conservative assumptions of the magnitude of residual stresses at the crack tip must be made. Here, plots were made for $\theta = \pi/2$ where the contribution from residual stresses to crack driving force is set equal to the maximum from the distribution in Fig. 14. These cases are denoted "worst case" in Figs. 35 to 37. It can be seen that in these cases the effect of residual stresses is overestimated according to BS 7910.

As mentioned linear interpolation was used, as L_r was not coincident for coincident increments in the simulation with residual stresses and the corresponding reference solution. The difference increase as L_r increase, thus, the error caused by interpolation also increase. However, the results are consistent and potential error caused by interpolation are assumed negligable at $L_r < 1$. Still, it can be seen some inconsistency at $L_r > 1$, which might have been caused by interpolation.

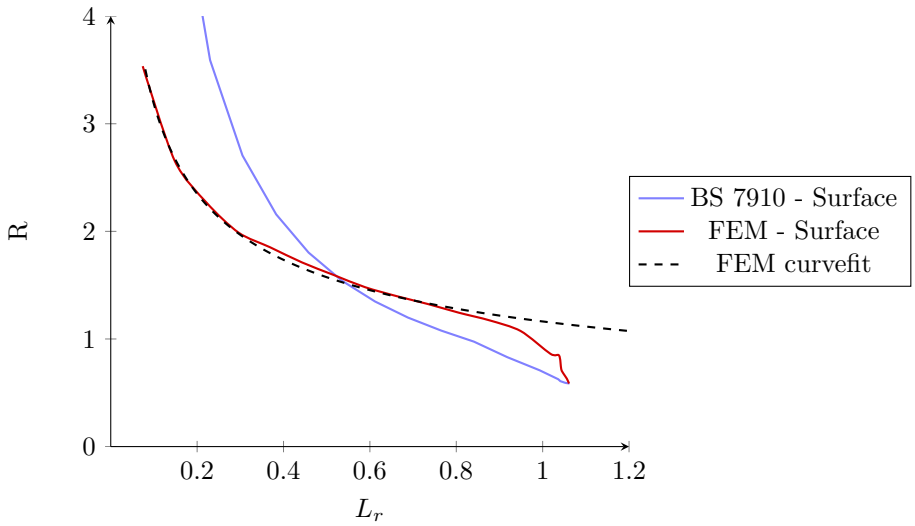

Figure 32: Effect of residual stresses in level 2B FAD for model 3 with crack depth, $a = 5$ mm, crack length 2c = 10 mm, surface $\theta = 0$

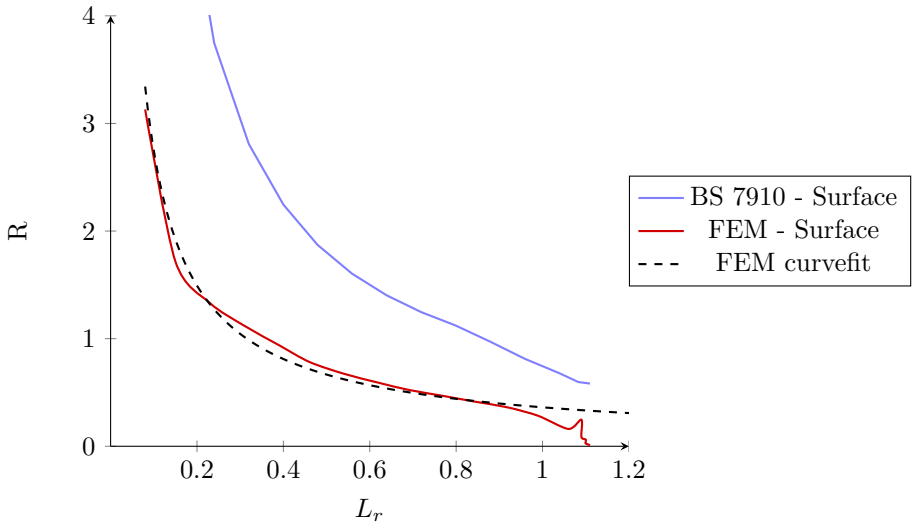

Figure 33: Effect of residual stresses in level 2B FAD for model 3 with crack depth, $a = 5$ mm, crack length $2c = 30$ mm, surface $\theta = 0$

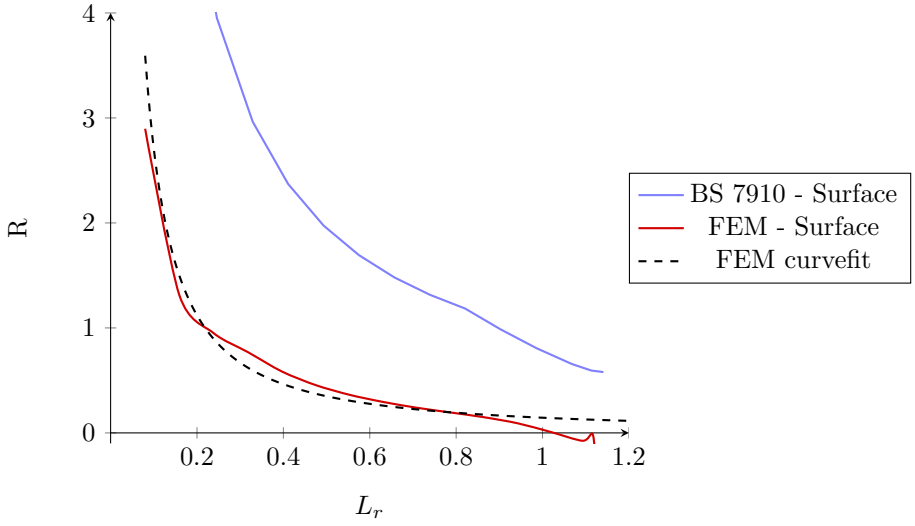

Figure 34: Effect of residual stresses in level 2B FAD for model 3 with crack depth, a = 5 mm, crack length 2c = 50 mm, surface $\theta = 0$

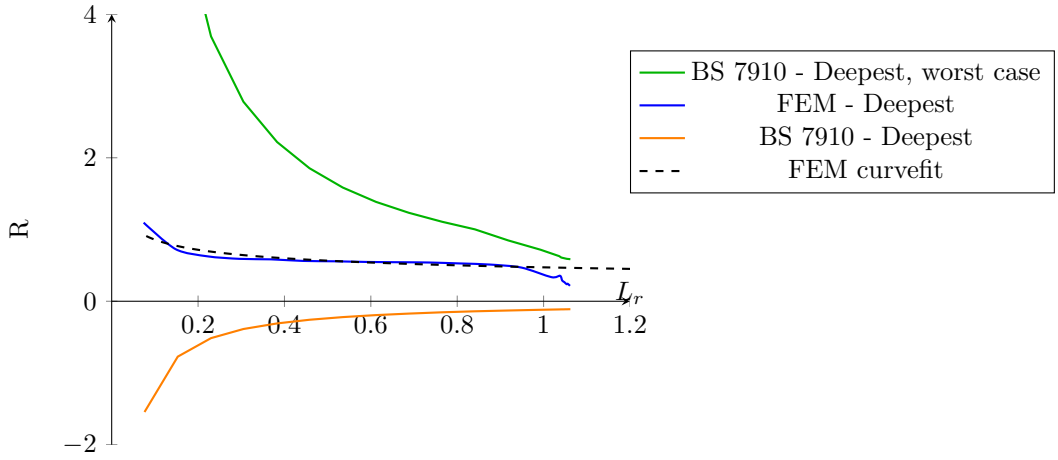

Figure 35: Effect of residual stresses in level 2B FAD for model 3 with crack depth, $a = 5$ mm, crack length $2c = 10$ mm, deepst point $\theta = \pi/2$

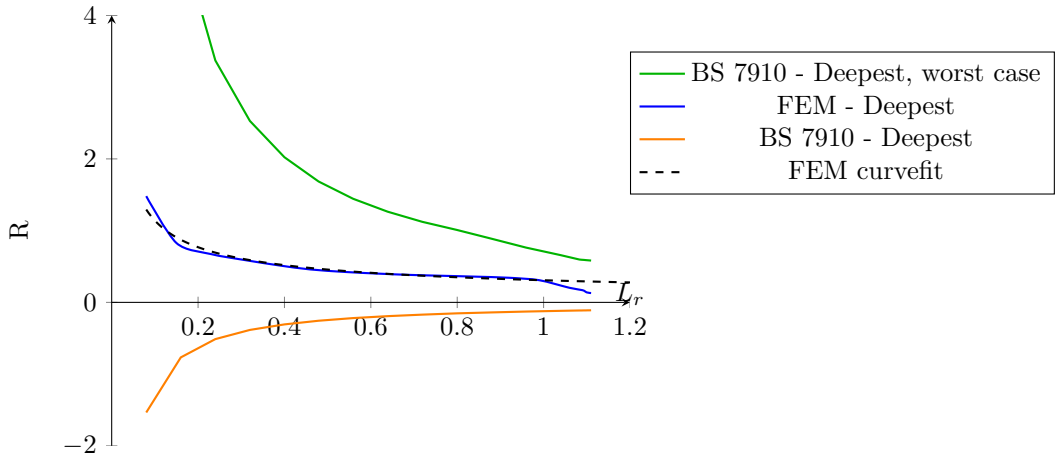

Figure 36: Effect of residual stresses in level 2B FAD for model 3 with crack depth, $a = 5$ mm, crack length $2c = 30$ mm, deepst point $\theta = \pi/2$

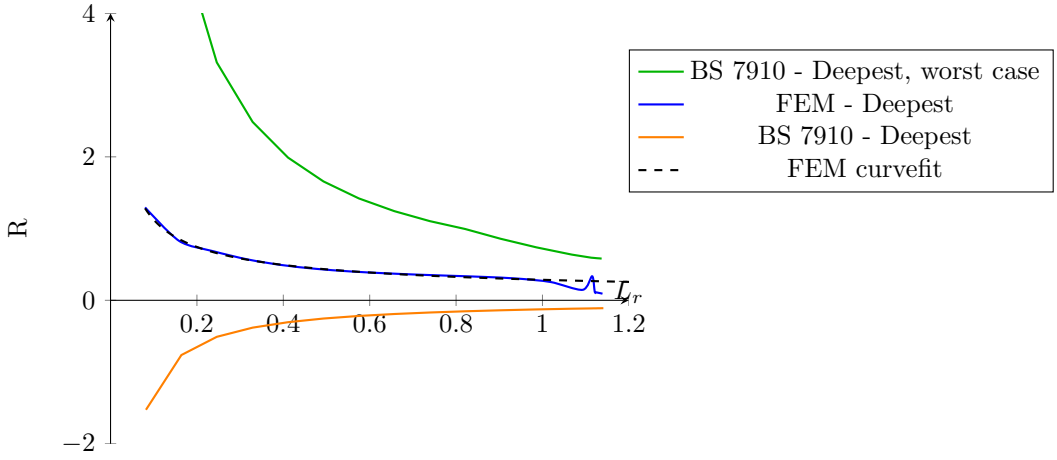

Figure 37: Effect of residual stresses in level 2B FAD for model 3 with crack depth, $a = 5$ mm, crack length $2c = 50$ mm, deepst point $\theta = \pi/2$

6.2 Effect of the a/c ratio on R

It can be seen from e.g. 32 to 34 that the effect of residual stresses, R, does not nessearily correspond with BS 7910. No universal difference between FEM and BS 7910 is seen. R seem todepend on the aspect ratio of the crack, a/c. This effect wil be discussed in this section.

In Section 6.1 the effect of residual stresses were shown in diagrams, where the corresponding solution according to BS 7910 also was included. As noted, the effect of residual stresses, R, does not only seem to be a function of L_r, but also of a/c. Thus, it it relevant to compare R as a function of L_r for different aspect ratios a/c. By plotting the results for different a/c ratios on the same diagram, shown in Fig. 38 to 41, the effect can be shown. Note that some of the curves shown here are the same as shown in in Section 6.1. All cracks shown here have the same depth $a = 5$ mm, while crack lengths are $2c = 10 - 50$ mm. Assessment both at the surface- and deepest point are relevant, as noted.

6.2.1 Assessment at the surface point, $\theta = 0$

It can be seen that R as a function of L_r decrease as the aspect ratio a/c decrease, according to FEM at the point where the crack front intersects the surface, $\theta = 0$. The effect of a/c on R is also very significant. According to BS 7910 however, this effect is different, i.e. R becomes greater as a/c increase, and the effect if less significant. This can be seen from Figs. 38 and 39. Lower R for lower a/c might be explained by, Eq. (23) and Eq. (24), which decide the magnitude of the stress intensity as a function of the position on the crack front. It can be seen that the stress intensity is greatest at $\theta = \pi/2$ when $a < c$, as is the case for model 3. It can also be seen that R is positive at $\theta = \pi/2$ even though the stresses are negative at this point. An explaination may be that the residual stresses are somehow redistributed as the crack is introduced. The difference in stress intensity for $\theta = 0$ and $\theta = \pi/2$ increase as a/c dacrease. This may be the explaination of why R as a function of L_r decrease as a/c decrease.

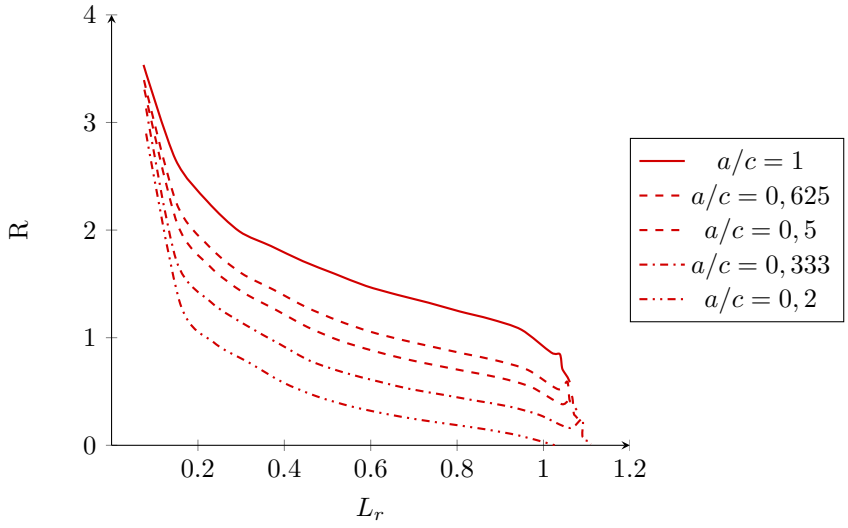

Figure 38: Effect of residual stresses in level 2B FAD for model 1/3 with crack depth, $a = 5$ mm, crack length $2c = 10 - 50$ mm, surface $\theta = 0$

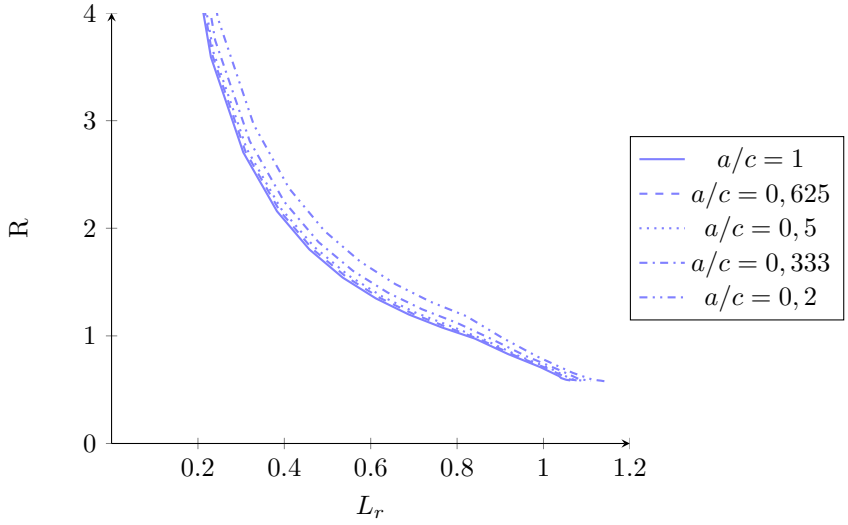

Figure 39: Effect of residual stresses in level 2B FAD, according to BS 7910 for model 1/3 with crack depth,$a = 5$ mm, crack length $2c = 10 - 50$ mm, surface $\theta = 0$

6.2.2 Assessment at the deepest point $\theta = \pi/2$

As there are compressive residual stresses at the deepest point of the crack, BS 7910 dictates that the contribution from residual stresses to crack driving force is negative, i.e. R is negative. Results from FEM however, suggests the opposite, i.e. that R is positive. As mentioned in the latter sction, the magnitude of the stress intensity, given by Eq. (23) to Eq. (24), is greatest at $\theta = \pi/2$. It seems that the variation of stress intensity over the crack front is not only valid for external loading, but also for residual stresses. BS 7910 however, suggests that the stress distribution from the uncracked plate is used. As there are compressive residual stresses at $\theta = \pi/2$, $\rho = 0$ for all values of L_r. Hence, R as a function of L_r is conincident for all a/c.

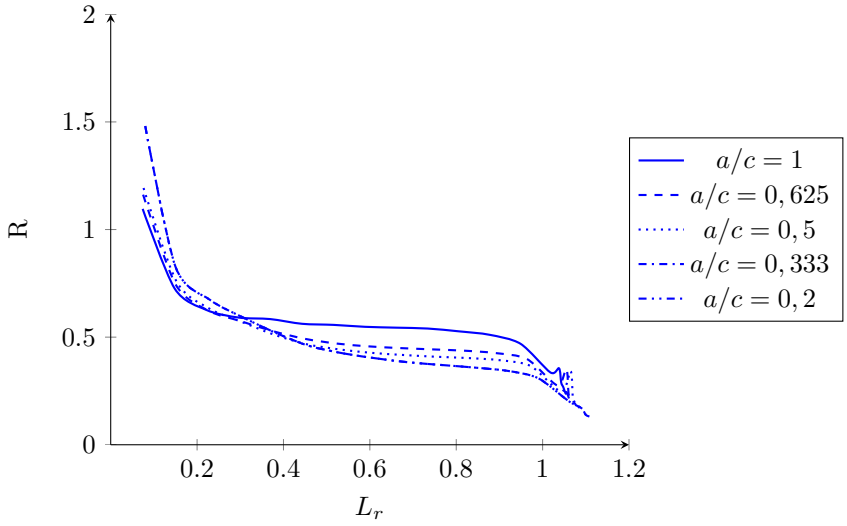

Figure 40: Effect of residual stresses in level 2B FAD for model 3 with crack depth, $a = 5$ mm, crack length $2c = 10 - 50$ mm, deepst point $\theta = \pi/2$

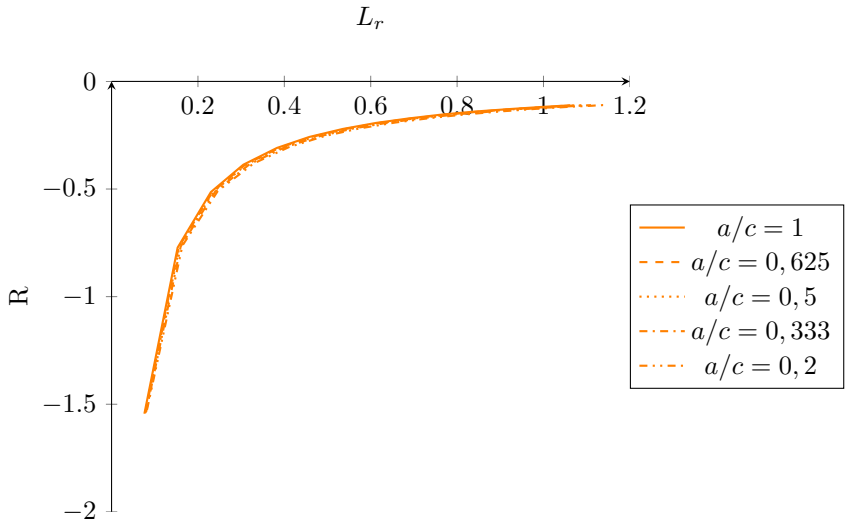

Figure 41: Effect of residual stresses in level 2B FAD, according to BS 7910 for model 1/3 with crack depth, $a = 5$ mm, crack length $2c = 10 - 50$ mm, deepst point $\theta = \pi/2$

6.3 The effect of hot cracks

As mentioned BS 7910 does not distinguish between hot and cold crack. Recall Tabs. 1 and 2. A cold crack is a crack introduced after residual stresses, while a hot crack is a crack that is already present at the time the residual stresses are introduced. A hot crack can e.g. be a welding defect and the results deviate to some degree from the results from cold cracks. Hot cracks with depth $a = 5$ mm and length $2c = 10 - 50$ mm were simulated in FEM.

6.3.1 Effect on R

The effect of hot- vs cold cracks for crack driving force at the surface point of the cracks is shown in Figs. 42 to 47. It can be seen that the contribution from residual stresses to crack driving force is somehow greater for hot cracks than for cold cracks, i.e. R is higher for the same L_r. However, the difference in R is not severe. It can also be seen that as the crack length increase, the difference becomes less significant.

At $\theta = 0$, R is in the range $\sim 20- \sim 30\%$ higher for hot cracks at $L_r = 0$ and decrease to $> 10\%$ higher as L_r approach 1. At the deepest point $\theta = \pi/2$, R is $\sim 15- \sim 50\%$ higher at $L_r = 0$, the difference here also de crease and is $> 10\%$ higher as L_r approach 1. It must als be mentioned that the difference in R for hot and cold cracks depend on the crack length c, as the crack depth a is kept constant. Greater difference in R is seen for shorter cracks.

Note the differences mentioned here are difference in R and not in the fracture ratio $\sqrt{\delta_r}$ or K_r. Recall Section 6.1. R is the the magnitude of the contribution to residual stresses to crack driving force, which deacrease as L_r increase.

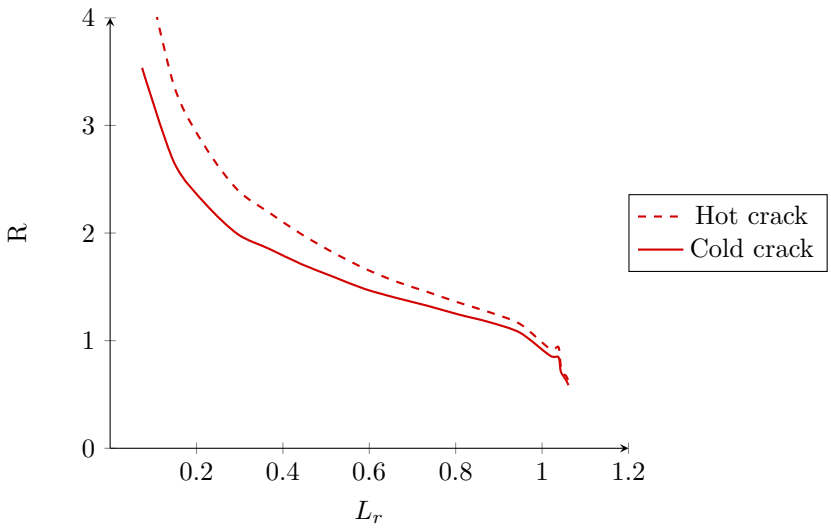

Figure 42: Effect of cold- vs hot cracks, model 3 with crack depth, $a = 5$ mm, crack length $2c = 10$ mm, surface $\theta = 0$

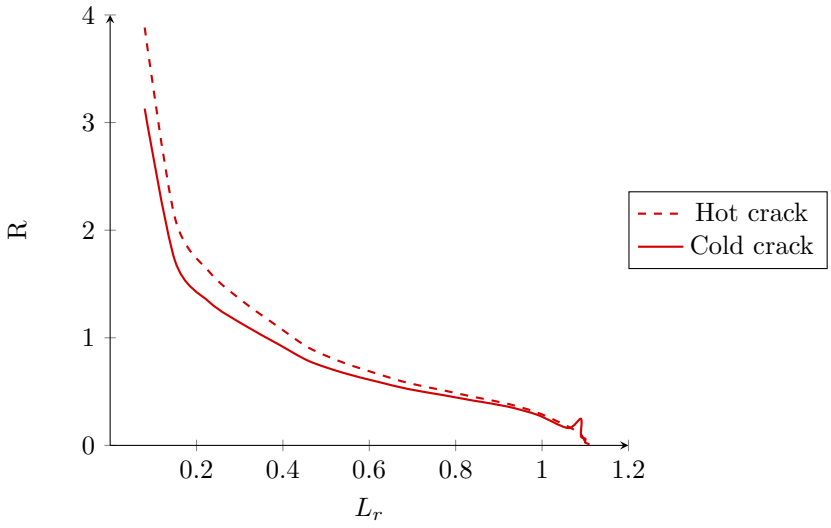

Figure 43: Effect of cold- vs hot cracks, model 3 with crack depth, $a = 5$ mm, crack length $2c = 30$ mm, surface $\theta = 0$

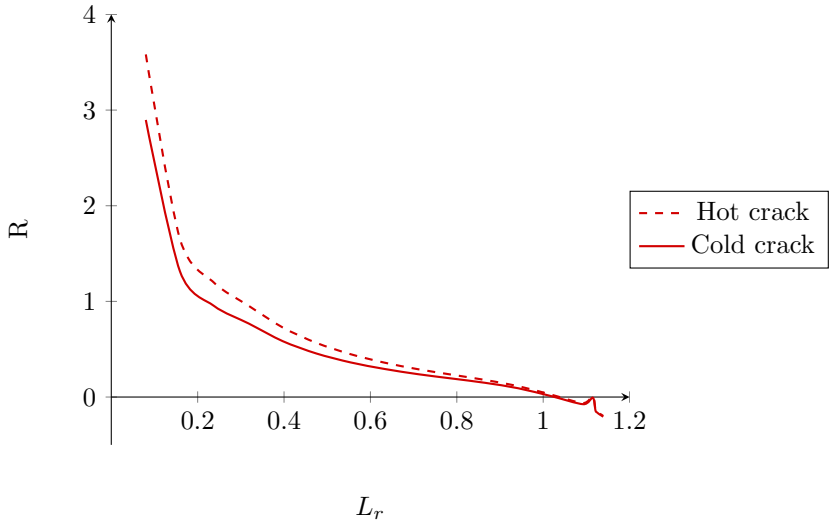

Figure 44: Effect of cold- vs hot cracks, model 3 with crack depth, $a = 5$ mm, crack length $2c = 50$ mm, surface $\theta = 0$

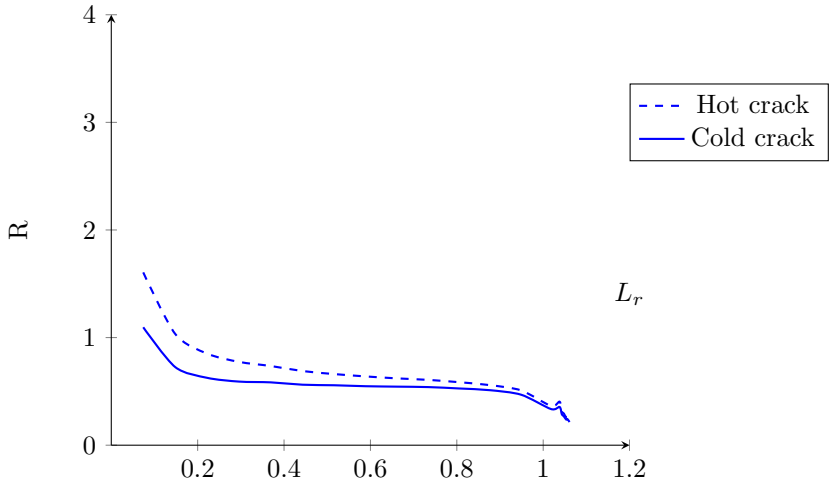

Figure 45: Effect of cold- vs hot cracks, model 3 with crack depth, $a = 5$ mm, crack length $2c = 10$ mm, deepst point $\theta = \pi/2$

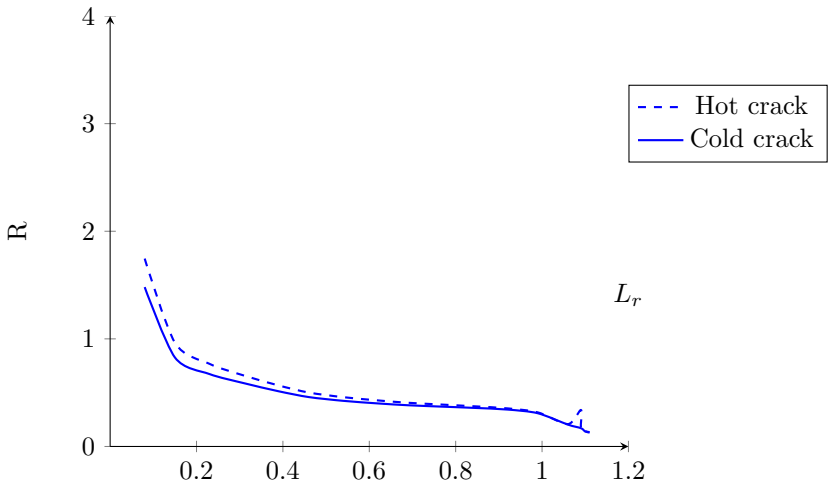

Figure 46: Effect of cold- vs hot cracks, model 3 with crack depth, $a = 5$ mm, crack length $2c = 30$ mm, deepst point $\theta = \pi/2$

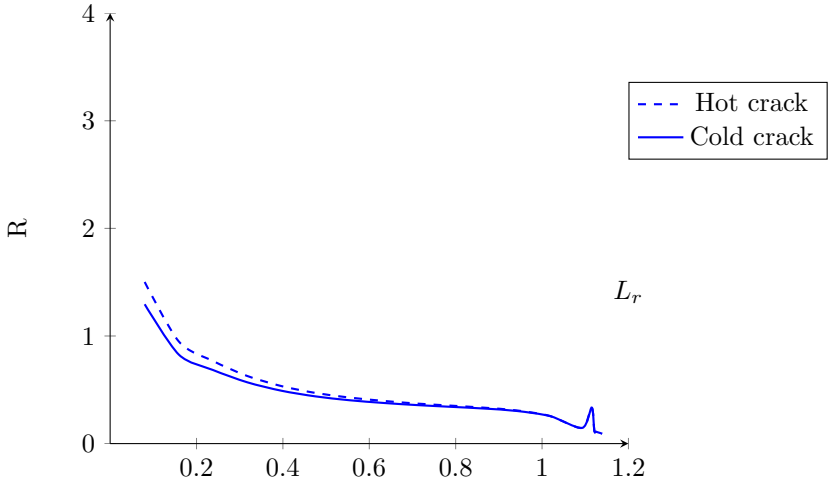

Figure 47: Effect of cold- vs hot cracks, model 3 with crack depth, $a = 5$ mm, crack length $2c = 50$ mm, deepst point $\theta = \pi/2$

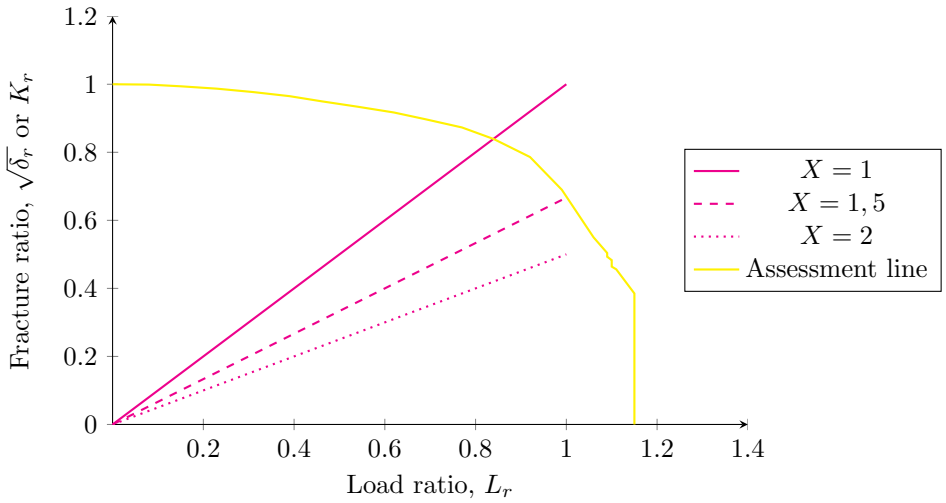

Figure 48: Effect of X on fracture ratio

6.4 Input to calculations according to BS 7910

As noted, the level 2B FAD analysis is presented in this work. The results are also implemented in the FAD diagrams. However, this analyses is based in certain parameters that are put into the equations.

6.4.1 Effect of X on fracture ratio

Recall Eq. (5), where $X = 1,5$ is used in this work. This value is assumed to be approximately correct in cases studied here, judging by the gradients of the load paths. However, X may be different in other cases, e.g. different material properties, geometry, etc. BS 7910 states that X is usually in the range of 1 and 2 depending of geometry, constraint and stain hardening of the material. BS 7910 allows X to be determined by structural analysis, and dictates that $X = 1$ if other value is not determined by the analyses. It can be seen form Fig. 48 that X has a significant effect on the load path. Note that the load paths in Fig. 48 is plotted according to $K_r = L_r/X$ in order to illustrate the effect of X. As X may have a significant impact on the load capacity, thorough investiagtion of X should be done for cases studied. Assuming $X = 1$ may lead to exessively conservative estimates of load capacity.

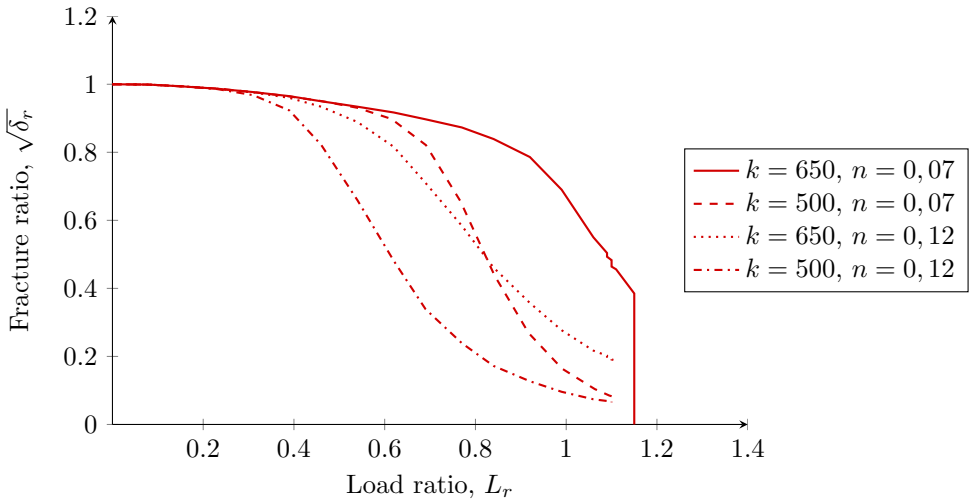

Figure 49: FAD Level 2B

6.4.2 Effect of stess - strain curve on the assessment line

It can be seen from Fig. 49 that the material stress strain relationship is very significant for the assessment line according to BS 7910 FAD level 2B. In BS 7910 the effect of residual stresses is added to the contribution from external loading. In addition, ρ is included in the fracture ratio as highest at zero load. If a material with higher exponent of lower multiplier in the stress - strain relationship was considered, the effect f resiudal stresses on load capacity would be more significant. In Eq. (26) $k = 650$ and $n = 0,07$. However, looking at e.g. Fig. 20 and 16 it can be seen that BS 7910 is only conservative at low values of L_r for deep cracks.

6.5 Validity of FEM analyses

FEM analyses is a method for detemining an approximate solution to a complex problem by discretization into elements with known solutions. Error may occur as FEM approximates results which is relevant to discuss here.

6.5.1 Convergence

A FEM model with a coarse mesh will have a certain degree of error. This error vanishes as the mesh is refined and element size decrease. Reducing element size will yield more accurate results, i.e. closer to the real solution. Fig. 50 shows

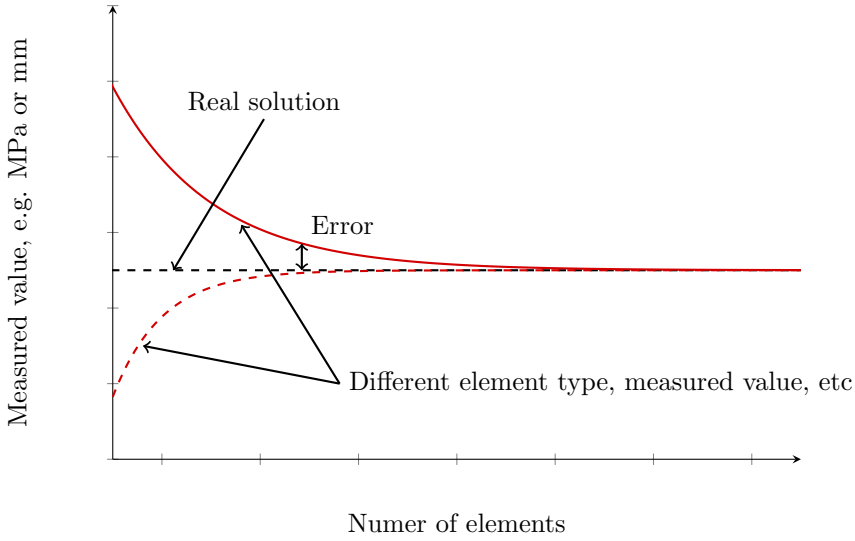

Figure 50: Illustration of convergence

examples of relations between results from FEM and number of elements. Note that this figure is an illustration with no values assigned. Relation between number of elements and error may also be different. It can be seen however, that the error vanish as number of element increase, in which case element size decrease.

In this work a convergence study was carried out for model 1 with crack depth $a = 10mm$. The same, or close to the same, element size was used in the same regions in all models. Therefore, it is assumed that convergence check is not necessary for all models and crack sizes. The convergence study was performed by changing the element size in different regions of the "original" mesh, one at a time, and running one simulation for each region that was changed. In total five different meshes were tested and results compared. The values that were measured were the reaction force vs the displacement of the node, closest to the crack tip at the surface. I.e. the same as for the simulations presented in section 5. The full results from the convergence study is shown in Annex B

It can be seen from Fig. 51 that changing the element size throughout the model has little effect on the results. Hence, convergence of models used are judged as likely and error in results as a cause of element size it assumed ~ 0.

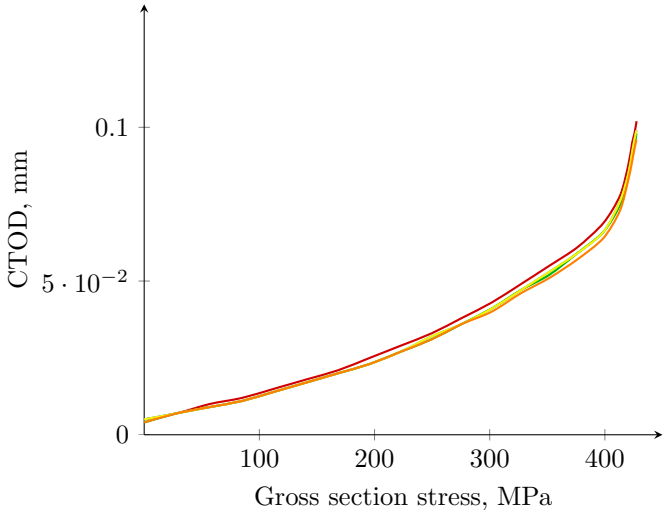

Figure 51: Results from convergence study of model 1,$a = 10$ mm

6.5.2 Definition of CTOD in FEM

It can be seen from e.g. Fig. 18 that the load paths according to the FEM analyses and LEFM are not coincident. This is probabily due to a combination of multiple factors, which will be discussed here.

As shown in Fig. 13 the CTOD in the FEM analyses is defined as the displacement of the node closest to the crack tip in the loading direction (U1), multiplied by two the due to symmetry. The crack that is modeled is an infinately sharp crack. This may cause high local plasticity at the crack tip at early increments and affect the CTOD significantly. As seen in e.g. Fig 18 the load path suddenly rise at the first increment, causing significantly higher fracture ratio than what LEFM pedicts. Since the load path according to FEM in these cases are corrected by mutliplying with the assessment line, which depends on the stress-strain curve of the material, they should be coinident with the load path according to LEFM. Still, the curves are not coincident. It must be mentioned however, that this effect is only seen in cases where there are no residual stresses.

6.5.3 FAD level

As mentioned, level 1,2 and 3 FAD analyses are available in BS 7910, with increasing level of accuracy. In this work the level 2B analysis is used with the

assessment line given by Eq. (12), which depends solely on the material stress-strain curve. However a level 3C analysis allows the assessment line to be plotted as a function of both the material properties and geometry of the component of interest, as well as the crack shape. In the level 3C assessment the true realtionship between LEFM and FEM is used to plot the assessment line, given in Eq. (32). Where J_e and δ_e are the elasticly calculated driving forces and J and δ are the true driving forces according to e.g. FEM. Note that BS 7910 only yield the left side and middle of Eq. (32). However, J and δ are proportional which yield the right side of the equation.

$$K_r = \sqrt{\frac{J_e}{J}} = \sqrt{\frac{\delta_e}{\delta}} \tag{32}$$

In this work however, using a level 3C analysis proved inconvenient, as the ratio between δ_e and δ seemed to be distorted at low loads. Still, the effect of resiudal stresses are taken form models with the exact same mesh. I.e. the model with corresponding reference model. A perpahs more illustrative way to show the concept of the level 3C FAD analysis is in Figs. 52 and 53. Fig. 53 is plotted based on Fig. 52. The level 3C assessment line is the square root of the ratio between crack driving force according to LEFM and FEM. It can be seen from Fig. 52 that the difference between LEFM and FEM is very significant at low load, but vanish as load increase. In idea for further work on this subject might include building a model where crack driving force according to LEFM and FEM are coincident at low loads in order to get a convenient level 3C assessment line. An initial notch at the crack tip might help in correcting this error.

6.5.4 Validity of loading paths from FEM

As mentioned, the load path for the reference models were not coincident with the corresponding solution according to BS 7910. Recall that all loading paths from FEM were multiplied by the assessment line level 2B. As loading path are not coincident for reference models according to FEM and BS 7910, the level 2B assessment line can not be interpreted as truly valid. Hence, no conclusion can be made on whether or not a fracture assessment according to BS 7910 is overly conservative. However, the effect of residual stresses is the main focus of this work and it's effect is more shown clearly.

6.5.5 Effect of residual stresses

The effect of residual stresses in this work is investigated by comparison of FEM models with residual stresses and reference models without residual stresses. Recall e.g. Figs. 32 to 34 where the effect is quantified. Even though the load

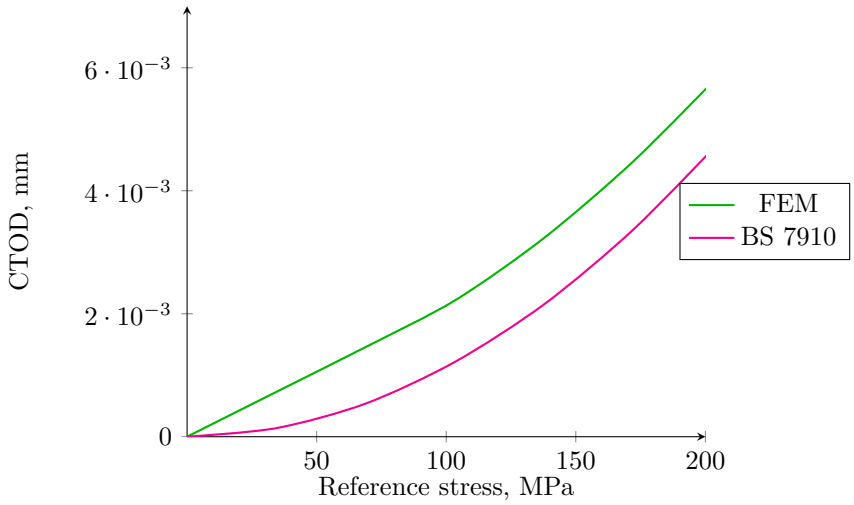

Figure 52: CTOD - Reference stress, reference model 3, crack depth $a = 5$ mm, crack length $2c = 50$ mm, deepest point

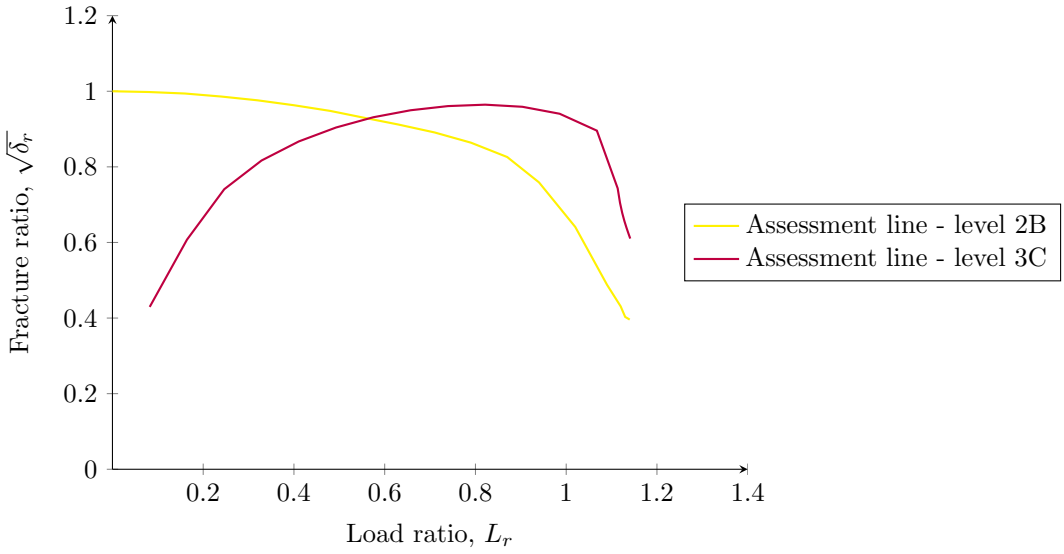

Figure 53: Level 2B and 3C assesment lines for referenace model 3 with crack depth, $a = 5$ mm, crack length $2c = 30$ mm deepest point, $\theta = \pi/2$

paths for reference models are not coincident with the load path according to BS 7910, the effect of residual stresses are assumed to be reasonable Models with residual stresses were compared to reference solutions where the models weere the exact same. I.e. the geometry, mesh and BCs of the reference model were identical. Hence the effect of residual stresses as shown is assumed to be credible. Small error due to linear interpolation however, might have caused minor errors at certain points. E.g. small jumps in the effect of residual stresses can be seen at high L_r for Fig. 37. Still, consistency is seen throughout the results which prove a basis for conclusions.

6.6 Residual stresses equal to the material yield strength

In BS 7910 the residual stresses may be assumed uniform and equal to the material yield strength. In this work, however, the stress field in the cracked models were not uniform. Neither were the residual stresses close to the yield strength, with a maximum stress of $\sim 0,6 * \sigma_Y$. It is not within the scope of this work to determine the the real distribution of residual stresses. Thus, no conclusion could be drawn on whether or not assuming the residual stresses to be equal to the yield strength is overly conservative or not.

6.7 Future work

This work has studied how residual stresses affect the crack driving force in a plate with residual stresses. However, the scope was limited in order to meet the required timeframe of the work.

6.7.1 Crack aspect ratio

The main focus of this work is on surface cracks. Crack with depth $a = 5$ mm and length up to $2c = 50$ mm were investigated. The deepest point of a crack with depth 5 mm is in an area with compressive residual stresses. Thus, future work may focus on more shallow cracks with the deepest point located in an area with tensile residual stresses. Smaller cracks, i.e. cracks with lower a or c, are more difficult to detect using non-destructive testing. Hence, small cracks that pose danger of fracture are of great importance in integrity assessments. If more knowledge about such cracks were to be obtained, it would prove a better basis for inspection and repair routines.

6.7.2 Distribution of residual stresses

The cases investigated in this work were limited to one distribution of residual stresses. However, the distribution in a real structure depend on a number of

different parameters, e.g. material properties geometry and heat input. BS 7910 outlines the range where the distribution of residual stresses usually is. This range is vast. Hence, studying the effect of different distributions of resiudal stresses would be of relevance.

6.7.3 Determination of R

In this work, the effect of residual stresses has been quantified as the dimensonless parameter R. It is seen that R depend on the crack aspect ratio, crack depth and shape of crack. It is however assumed that a number of additional factors affect R. The level of residual stresses. material properties and plate thickness are among the factors that may affect R. Hence, there is motivation of thorough study of the factors affecting R. If knowledge were to be gained, the crack driving force in a component with residual stresses might be determined by R and the crack driving force for a reference solution.

6.7.4 Position of crack

The scope of this work was limited to cracks parallel to the crack direction in the centre of the weld. However the distribution of residual stresses in the welding direction is different from the distribution used here. Hence future work could investigate cracks oriented normal to the welding direction.

7 Conclusion

In this work, the effect of residual stresses on crack driving force has been invesitgated by comparing the crack driving force from a model with residual stresses to a reference solution, without residual stresses. The two models were identical. All models were plates 1200×1200 mm with thickness 25 mm. Surface cracks with $a = c$ and depths of 5 - 20 mm, $a = 5$ mm and $2c = 30 - 50$ mm and through thickness cracks with $a \leq 25mm$ were investigated. The results were plotted in FAD level 2B according to BS 7910, which is a common standard for fracture assessments. The effect of residual stresses is quantified as R which is the difference in fracture ratio between the model with residual stresses and the correspeonding reference solution, divided by the frature ratio for the reference solution. This is compared to how residual stresses are treated in fracture assessments according to BS 7910. Based on work performed, the following concludions can be drawn.

- The effect of residual stresses R decrease as L_r increase.
- The effect of resiudal stresses R is usually higher according to BS 7910 than what is computed from FEM.
- BS 7910 may overestimate the effect of residual stresses increasingly as crack depth, a, or crack length $2c$ increase.
- BS 7910 may undestimate the effect of residual stresses for small cracks
- In cases where there are compressive residual stresses at the crack tip, BS 7910 may underestimate the effect of residual stresses. This may be explained by the distribution of residual stresses which gives tension in the surface and compression near the mid thickness. In practice however, limited knowledge about the real distribution of residual stresses may lead to conservative assumptions of the magnitude of residual stresses at the crack tip, which again leads to conservative fracture assessments.
- The effect of residual stresses, R, is slightly higher for hot cracks than cold cracks. However, the difference vanish as load, L_r, increase.

Acknowledgements

Completing this work and achieving my Master's degree would not have been possible without the assistance and guidance of several persons as NTNU and SINTEF. First and foremost, I want to acknowledge professor Mons Hauge, who has been my main supervisor during this semester, giving superb guidance, his sincere opinion as well as showing true interest in my work. Always having a positive, calm and down to earth attitude. My gratitude is also owed to professor Christian Thaulow, who was the first person to elicit my interest for Arctic Materials, also letting me present my progress weekly at his research gruop meetings and providing useful and positive feedback. I also wish to acknowledge Dr. Xiaobo Ren at SINTEF for taking his time to lecture me in using Abaqus for fracture assessments as well as proving me with guidance throughout the semester. I am also grateful to Håkon A Holm Gundersen and Jørn Skogsrud who saw the necessity of a powerful computer to run my simulations and eventually provided me with access to the supercomputer Vilje on NTNU. The two latter persons as well as Nousha Kheradmand owe my gratitude for letting me use their office from time to time. I also wish to acknowledge everyone in professor Christian Thaulow's group for positive and contructive feedback. The Master's students at room 212 are also acknowldged for maintaining a great working environment throghout this semester.

References

[1] William Magnor. Arctic steels - guidelines, modeling and fracture assessment, December 2012.

[2] M. Hauge. Arctic offshore materials and platform winterisation. pages 278–282, June 2012.

[3] A.M. Horn and M. Hauge. Material challenges for arctic offshore applications, a reliability study of fracture of a welded steel plate based on material toughness data at -60 °c. pages 393–401, 2011. cited By (since 1996) 0.

[4] Materials challenges on arctic areas. Poster, 11 2011.

[5] A.M. Horn, E. Østby, M. Hauge, and J.-M. Aubert. Robust material qualification for arctic application. pages 290–296, June 2012.

[6] International Organization for Standardization. Iso 19902:2007 petroleum and natural gas industries - fixed steel offshore structures, 2007.

[7] Standard Norge. Ns-en 10025 hot rolled products of steel, part 1: General technical delivery conditions, January 2005.

[8] Application to the norwegian research counsil for the arctic materials project.

[9] Arctic materials ii scope, January 2013.

[10] Arctic material kmb project guideline draft, May 2012.

[11] British Standards. Bs 7910 guide to methods for assessing the acceptability of flaws in metallic structures, 2005.

[12] XB Ren, ZL Zhang, and B Nyhus. Effect of residual stresses on the crack-tip constraint in a modified boundary layer model. *International Journal of Solids and Structures*, 46(13):2629–2641, 2009.

[13] Xiaobo Ren. *Effect of welding residual stresson fracture*. PhD thesis, Norwegian University of Science and Technology, Department of Structural Engineering, 2010.

[14] Xudong Qian and Tieping Li. Residual stress effects on the crack-front constraints for surface cracks in pipes. *ASME Conference Proceedings*, 2010(49132):123–131, June 2010.

[15] Xudong Qian and Tieping Li. Effect of residual stresses on the linear-elastic ki–t field for circumferential surface flaws in pipes. *Engineering Fracture Mechanics*, 77(14):2682 – 2697, 2010.

[16] MI Onsøien, M MHAMDI, and OM Akselsen. Residual stresses in weld thermal cycle simulated specimens of x70 pipeline steel. *Welding Journal*, 89, 2010.

[17] P.J. Bouchard. Validated residual stress profiles for fracture assessments of stainless steel pipe girth welds. *International Journal of Pressure Vessels and Piping*, 84(4):195 – 222, 2007.

[18] D.J. Hughes, P.J. Webster, and G. Mills. Ferritic steel welds - a neutron diffraction standard. *Materials Science Forum*, 404-407:561–566, 2002. cited By (since 1996)9.

[19] M.L. Martinez-Perez, F.J. Mompean, J. Ruiz-Hervias, C.R. Borlado, J.M. Atienza, M. Garcia-Hernandez, M. Elices, J. Gil-Sevillano, R.L. Peng, and T. Buslaps. Residual stress profiling in the ferrite and cementite phases of cold-drawn steel rods by synchrotron x-ray and neutron diffraction. *Acta Materialia*, 52(18):5303–5313, 2004. cited By (since 1996)39.

[20] W. Woo, V.T. Em, B.S. Seong, P. Mikula, and G.B. An. Residual stress determination in a thick ferritic steel weld plate using neutron diffraction. *Journal of Materials Science*, 47(14):5617–5623, 2012. cited By (since 1996) 0.

[21] SINTEF. http://www.sintef.no/projectweb/resia/some-project-results/the-weldsims-model/.

[22] Anderson. *Fracture Mechanics: Fundamentals and Applications*. CRC Press, third edition, 2005.

[23] Z.L. Zhang, M. Hauge, and C. Thaulow. Two-parameter characterization of the near-tip stress fields for a bi-material elastic-plastic interface crack. *International Journal of Fracture*, 79(1):65–83, 1996. cited By (since 1996) 37.

List of Figures

List of Tables

A Stress - strain curve for material used

E	207000

Sig-y	**420**
eps_0	0,002029
n	**0,07**

X70 stress strain kurve

Pl strain [mm/mm]	True stress MPa
0	500
0,0001	501,4218
0,0002	502,792
0,0003	504,1143
0,0004	505,3921
0,0005	506,6284
0,0006	507,8258
0,0007	508,9869
0,0008	510,1138
0,0009	511,2085
0,001	512,273
0,0012	514,3177
0,0015	517,1956
0,0018	519,8753
0,002	521,5649
0,0025	525,4961
0,003	529,0717
0,0035	532,3524
0,004	535,3847
0,0045	538,2047
0,005	540,8411
0,0055	543,3171
0,006	545,6517
0,007	549,9573
0,008	553,8568
0,009	557,4226
0,01	560,7089
0,012	566,6019
0,015	574,1501
0,02	584,3841
0,03	599,6705
0,035	605,7224
0,04	611,064
0,05	620,1863
0,06	627,8133
0,07	634,3782
0,08	640,1484
0,09	645,3007
0,1	649,9585
0,15	668,3009
0,2	681,706
0,25	692,322

X70 stress strain kurve

Pl strain [mm/mm]	True stress MPa
0	0
0,0012077	250
0,0024155	500
0,0025223	501,4218
0,0026289	502,792
0,0027353	504,1143
0,0028415	505,3921
0,0029475	506,6284
0,0030533	507,8258
0,0031589	508,9869
0,0032643	510,1138
0,0033696	511,2085
0,0034747	512,273
0,0036846	514,3177
0,0039985	517,1956
0,0043115	519,8753
0,0045196	521,5649
0,0050386	525,4961
0,0055559	529,0717
0,0060718	532,3524
0,0065864	535,3847
0,0071	538,2047
0,0076128	540,8411
0,0081247	543,3171
0,008636	545,6517
0,0096568	549,9573
0,0106756	553,8568
0,0116929	557,4226
0,0127087	560,7089
0,0147372	566,6019
0,0177737	574,1501
0,0228231	584,3841
0,032897	599,6705
0,0379262	605,7224
0,042952	611,064
0,0529961	620,1863
0,0630329	627,8133
0,0730646	634,3782
0,0830925	640,1484
0,0931174	645,3007
0,1031399	649,9585
0,1532285	668,3009
0,2032933	681,706
0,2533446	692,322

0	0
0,0012077	250
0,0024155	443,69751
0,0025223	444,43611
0,0026289	445,15708
0,0027353	445,86135
0,0028415	446,54977
0,0029475	447,22311
0,0030533	447,88208
0,0031589	448,52736
0,0032643	449,15955
0,0033696	449,77923
0,0034747	450,38694
0,0036846	451,56837
0,0039985	453,26214
0,0043115	454,87097
0,0045196	455,9007
0,0050386	458,34116
0,0055559	460,61301
0,0060718	462,7394
0,0065864	464,73886
0,0071	466,62652
0,0076128	468,41485
0,0081247	470,11432
0,008636	471,73378
0,0096568	474,76185
0,0106756	477,54806
0,0116929	480,12978
0,0127087	482,53619
0,0147372	486,91166
0,0177737	492,61815
0,0228231	500,51279
0,032897	512,5782
0,0379262	517,42795
0,042952	521,73719
0,0529961	529,15024
0,0630329	535,39294
0,0730646	540,79414
0,0830925	545,55999
0,0931174	549,82847
0,1031399	553,69662
0,1532285	569,00154
0,2032933	580,2435
0,2533446	589,17197

0,3	701,1361	0,3033871	701,1361	0,3033871	596,59856
0,35	708,686	0,3534236	708,686	0,3534236	602,9683
0,4	715,2984	0,4034555	715,2984	0,4034555	608,55238
0,45	721,1866	0,453484	721,1866	0,453484	613,52861
0,5	726,498	0,5035097	726,498	0,5035097	618,02006
0,55	731,3388	0,553533	731,3388	0,553533	622,11553
0,6	735,7881	0,6035545	735,7881	0,6035545	625,88126
0,65	739,9063	0,6535744	739,9063	0,6535744	629,36799
0,7	743,7408	0,703593	743,7408	0,703593	632,61547
0,75	747,3294	0,7536103	747,3294	0,7536103	635,65546
0,8	750,7027	0,8036266	750,7027	0,8036266	638,5137
0,85	753,8859	0,853642	753,8859	0,853642	641,21141
0,9	756,9	0,9036565	756,9	0,9036565	643,76622
0,95	759,7625	0,9536704	759,7625	0,9536704	646,19301
1	762,4886	1,0036835	762,4886	1,0036835	648,50441
1,1	767,581	1,1037081	767,581	1,1037081	652,82292
1,2	772,2605	1,2037307	772,2605	1,2037307	656,79225
1,3	776,5913	1,3037516	776,5913	1,3037516	660,46633
1,4	780,6231	1,4037711	780,6231	1,4037711	663,88738
1,5	784,3959	1,5037894	784,3959	1,5037894	667,0891
1,6	787,9421	1,6038065	787,9421	1,6038065	670,0988
1,7	791,2881	1,7038226	791,2881	1,7038226	672,93893
1,8	794,456	1,803838	794,456	1,803838	675,6282
1,9	797,4646	1,9038525	797,4646	1,9038525	678,18234
2	800,3295	2,0038663	800,3295	2,0038663	680,61473

$$\sigma = \sigma_0 \left(1 + \frac{\bar{\varepsilon}^p}{\varepsilon_0}\right)^n$$

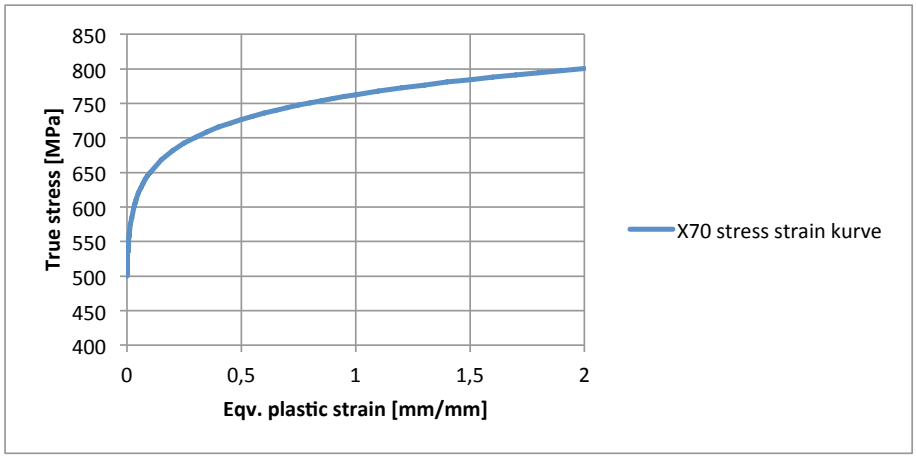

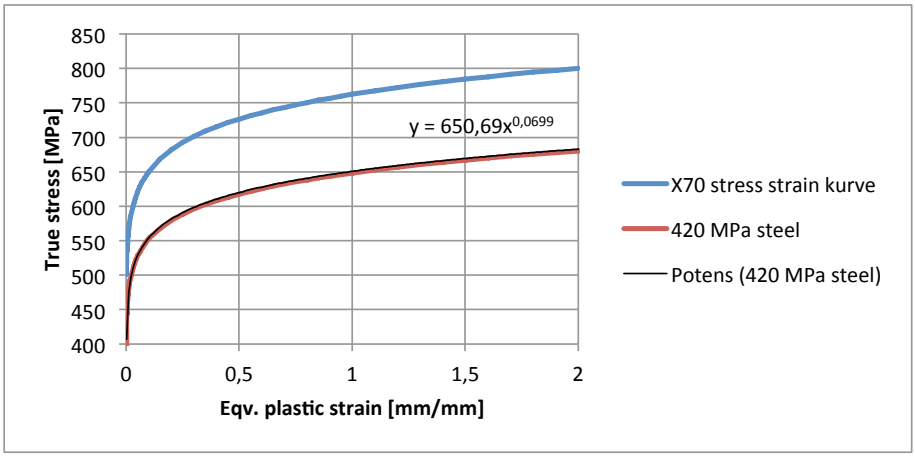

B Convergence study

Material properties			Plate geometry	
Yield strength (MPa)	420		Half plate length (mm)	200
Tensile/Yield ratio	1,2	Assumed	Half plate width (mm)	100
Tensile strength (MPa)	504		Plate thickness (mm)	25
Elastic modulus, E (MPa)	207000		Gross area (mm^2)	2500
Poisson factor, v	0,3		Crack depth, a (mm)	10
Effective E-modulus, E' MPa	227473		Crack length, c (mm)	10
CTODcrit	0,1	fornuftig verdi!	Net area (mm^2)	2421
χ	1,5	9,63b Anderson	a"	0,114285714
Kmat	119,7111909			
Lrmax	1,1			
Flow stress (MPa)	462			
Stress - strain curve				
Multiplier	650,69			
Exponent	0,0699			

Displacement of node closes to crack tip, mm

area	"Normal" mesh	crack front	front	ligament and surface
-2,42E-03	-2,26E-03	-2,24E-03	-0,00226631	-0,00222429
-3,57E-03	-0,00334394	-0,00331796	-0,00334785	-0,00329731
-0,00478714	-0,00447337	-0,00443975	-0,00447706	-0,00441906
-0,0060819	-0,0056809	-0,00563885	-0,00568461	-0,00564101
-0,00748171	-0,00699484	-0,00693743	-0,00699916	-0,00699488
-0,0090137	-0,00843816	-0,00837068	-0,00844147	-0,00844934
-0,0106875	-0,0100228	-0,00994401	-0,0100237	-0,0100143
-0,0125152	-0,0117474	-0,0116717	-0,0117488	-0,0116981
-0,014524	-0,0136631	-0,0135944	-0,0136601	-0,0135451
-0,0166971	-0,0157622	-0,0156873	-0,0157583	-0,01557
-0,0190661	-0,0180788	-0,0179943	-0,0180794	-0,017791
-0,0216501	-0,0206193	-0,0205222	-0,0206215	-0,020207
-0,0244518	-0,0233834	-0,023263	-0,0233859	-0,0228551
-0,0274717	-0,0263521	-0,0261878	-0,0263514	-0,0256681
-0,0306949	-0,0295447	-0,0293269	-0,0295457	-0,0286883
-0,0342706	-0,0331032	-0,0328782	-0,0331049	-0,0321263
-0,0390782	-0,0378532	-0,0375928	-0,0378521	-0,0367327
-0,0440043	-0,0426752	-0,0423545	-0,0426758	-0,0414219
-0,0473731	-0,0459565	-0,04551	-0,0459602	-0,04462
-0,0491739	-0,0477681	-0,0472317	-0,0477724	-0,0463866
-0,0509019	-0,0494715	-0,0488991	-0,049476	-0,0480484

Reaction force, tension side, N

area	"Normal" mesh	crack front	front	ligament and surface
0	0	0	2,07E-13	-3,27E-13
-71339	-71308	-71272	-71308,4	-71305,4
-142248	-142198	-142140	-142198	-142196
-212745	-212698	-212612	-212698	-212697
-282789	-282723	-282592	-282724	-282723
-352314	-352137	-351982	-352137	-352137
-421261	-420990	-420809	-420990	-420991
-489572	-489208	-488995	-489208	-489210
-557156	-556671	-556443	-556671	-556672
-623896	-623384	-623131	-623384	-623384
-689661	-689145	-688858	-689145	-689146
-754320	-753881	-753578	-753882	-753881
-817738	-817380	-817045	-817380	-817381
-879825	-879482	-879141	-879482	-879483
-940464	-940107	-939818	-940107	-940107
-997437	-997102	-996879	-997103	-997104
-1033460	-1033110	-1033140	-1,03E+06	-1,03E+06
-1051190	-1051100	-1051190	-1,05E+06	-1,05E+06
-1059320	-1059280	-1059280	-1,06E+06	-1,06E+06
-1064170	-1064140	-1064130	-1,06E+06	-1,06E+06
-1068660	-1068620	-1068600	-1,07E+06	-1,07E+06

CTOD, mm

area	"Normal" mesh	crack front	front	ligament and surface
0,0048	0,0045	0,0045	0,0045	0,0044
0,0071	0,0067	0,0066	0,0067	0,0066
0,0096	0,0089	0,0089	0,0090	0,0088
0,0122	0,0114	0,0113	0,0114	0,0113
0,0150	0,0140	0,0139	0,0140	0,0140
0,0180	0,0169	0,0167	0,0169	0,0169
0,0214	0,0200	0,0199	0,0200	0,0200
0,0250	0,0235	0,0233	0,0235	0,0234
0,0290	0,0273	0,0272	0,0273	0,0271
0,0334	0,0315	0,0314	0,0315	0,0311
0,0381	0,0362	0,0360	0,0362	0,0356
0,0433	0,0412	0,0410	0,0412	0,0404
0,0489	0,0468	0,0465	0,0468	0,0457
0,0549	0,0527	0,0524	0,0527	0,0513
0,0614	0,0591	0,0587	0,0591	0,0574
0,0685	0,0662	0,0658	0,0662	0,0643
0,0782	0,0757	0,0752	0,0757	0,0735
0,0880	0,0854	0,0847	0,0854	0,0828
0,0947	0,0919	0,0910	0,0919	0,0892
0,0983	0,0955	0,0945	0,0955	0,0928
0,1018	0,0989	0,0978	0,0990	0,0961

Applied stress (S11), gross section, MPa				
"Normal" mesh	crack front	front	ligament and surface	
0,0	0,0	0,0	0,0	0,0
28,5	28,5	28,5	28,5	28,5
56,9	56,9	56,9	56,9	56,9
85,1	85,1	85,0	85,1	85,1
113,1	113,1	113,0	113,1	113,1
140,9	140,9	140,8	140,9	140,9
168,5	168,4	168,3	168,4	168,4
195,8	195,7	195,6	195,7	195,7
222,9	222,7	222,6	222,7	222,7
249,6	249,4	249,3	249,4	249,4
275,9	275,7	275,5	275,7	275,7
301,7	301,6	301,4	301,6	301,6
327,1	327,0	326,8	327,0	327,0
351,9	351,8	351,7	351,8	351,8
376,2	376,0	375,9	376,0	376,0
399,0	398,8	398,8	398,8	398,8
413,4	413,2	413,3	413,2	413,2
420,5	420,4	420,5	420,4	420,4
423,7	423,7	423,7	423,7	423,7
425,7	425,7	425,7	425,7	425,7
427,5	427,4	427,4	427,4	427,4

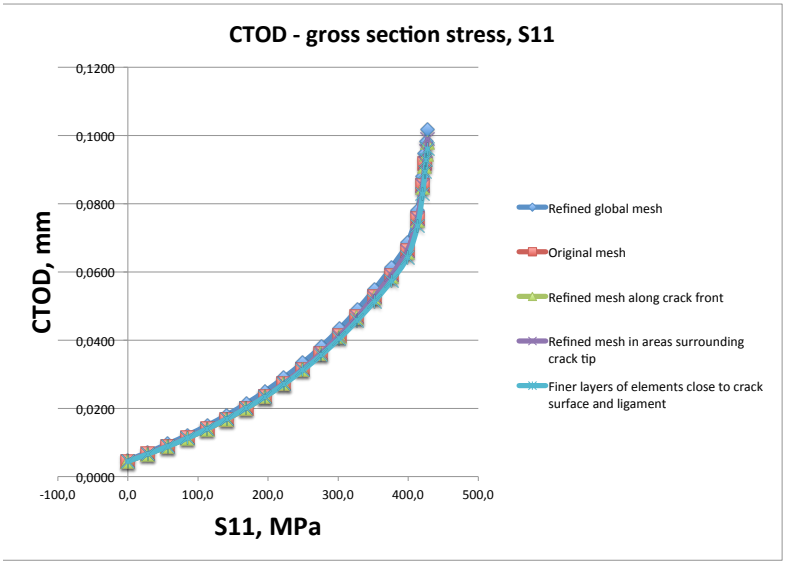

C Distribution of residual stresses

V-groove

Distance from surface	Stress (S11)	S11/YS	d/t
0	253,556	0,604	0,00
0,313437	237,78	0,566	0,01
0,626907	220,351	0,525	0,03
0,940414	201,344	0,479	0,04
1,25396	180,961	0,431	0,05
1,56754	159,494	0,380	0,06
1,88116	137,324	0,327	0,08
2,19482	114,882	0,274	0,09
2,5085	92,5941	0,220	0,10
2,82222	70,8539	0,169	0,11
3,13596	49,9923	0,119	0,13
3,44973	30,2567	0,072	0,14
3,76352	11,8127	0,028	0,15
4,07732	-5,24973	-0,012	0,16
4,39114	-20,9021	-0,050	0,18
4,70498	-35,1617	-0,084	0,19
5,01882	-48,0773	-0,114	0,20
5,33268	-59,7163	-0,142	0,21
5,64654	-70,1575	-0,167	0,23
5,96041	-79,4839	-0,189	0,24
6,27428	-87,7761	-0,209	0,25
6,58816	-95,1084	-0,226	0,26
6,90204	-101,55	-0,242	0,28
7,21592	-107,218	-0,255	0,29
7,55482	-112,198	-0,267	0,30
7,85679	-116,256	-0,277	0,31
8,12584	-119,299	-0,284	0,33
8,36556	-121,584	-0,289	0,33
8,57916	-123,301	-0,294	0,34
8,76947	-124,593	-0,297	0,35
8,93905	-125,564	-0,299	0,36
9,09014	-126,293	-0,301	0,36
9,22476	-126,83	-0,302	0,37
9,3252	-127,208	-0,303	0,37
9,42564	-127,491	-0,304	0,38
9,52608	-127,728	-0,304	0,38
9,62652	-127,921	-0,305	0,39
9,72696	-128,069	-0,305	0,39
9,72696	-128,173	-0,305	0,39
9,92784	-128,236	-0,305	0,40
10,0283	-128,256	-0,305	0,40
10,1287	-128,235	-0,305	0,41
10,2292	-128,158	-0,305	0,41
10,3638	-127,992	-0,305	0,41
10,5149	-127,716	-0,304	0,42
10,6844	-127,29	-0,303	0,43
10,8747	-126,673	-0,302	0,43
11,0883	-125,803	-0,300	0,44
11,328	-124,617	-0,297	0,45
11,5971	-123,019	-0,293	0,46
11,899	-120,909	-0,288	0,48
12,2379	-118,109	-0,281	0,49
12,6564	-114,46	-0,273	0,51
13,0748	-110,099	-0,262	0,52

13,4933	-105,194	-0,250	0,54
13,9118	-99,7632	-0,238	0,56
14,3302	-93,8159	-0,223	0,57
14,7487	-87,3651	-0,208	0,59
15,1671	-80,4104	-0,191	0,61
15,5856	-72,9634	-0,174	0,62
16,004	-65,0226	-0,155	0,64
16,4224	-56,6012	-0,135	0,66
16,8408	-47,7026	-0,114	0,67
17,2592	-31,4779	-0,075	0,69
18,7653	-0,15124	0,000	0,75
20,2713	40,7155	0,097	0,81
21,7771	83,2898	0,198	0,87
23,2826	124,808	0,297	0,93